Prospects for permanent magnets with non-critical rare earth elements in traction drive motors

M.J. Kramer
Ames Laboratory, Iowa State University, Ames IA 50011, USA

Jun Cui
Ames Laboratory, Iowa State University, Ames IA 50011, USA

Iver Anderson
Ames Laboratory, Iowa State University, Ames IA 50011, USA

Ikenna C. Nlebedim
Ames Laboratory, Iowa State University, Ames IA 50011, USA

It has been over a decade since the first crisis in the rare earth elements (REEs) supply chain [1]. While significant investments in exploring and developing new sources for REEs, alternatives to REE-based permanent magnets (PM), and new processing methods to reduce the more critical heavy REEs, much still needs to be done. Concern for climate change has accelerated regulations on internal combustion engines (ICE) and even planning outright bans of ICEs in many localities. Nd-Fe-B based PMs still provide the highest energy density in the temperature range (< 150°C) for most consumer and industrial applications. While current proven reserves for light REEs are sufficient in the near-term outlook for PM applications [2, 3], the supply chain for manufactures outside of China remains vulnerable. The heavy REE (Dy, Tb, Ho) needed for improved high temperature PM operations are scarce and getting scarcer [4] resulting in more uncertainty in price and availability. While there are many alternatives to the current Nd-Fe-B based PM alloys and some of these compounds can be utilized in PM-type traction motors, there is a penalty to the overall system performance. Substituting with these lower energy density alternative PMs will result in higher fossil fuel consumption in hybrid vehicles and lower driving range in all-electric vehicles for the same vehicle size. For all electric vehicles (AEV), loss in PM performance will require additional battery capacity. A 5% increase in battery capacity will cost nearly US$300, which is almost double the cost of the materials that goes into PM motors. Switching to lower performing PMs or to induction motors will greatly increase AEV [5]. This also means that the demand for the critical materials such as graphite, Li, Ni, Mn, Co will increase more rapidly.

The solutions are 1) develop a new PM without critical elements with performance matching Nd-Fe-B based PM, 2) develop new motor topologies that utilized characteristics of current non-critical PMs more efficiently, and/or 3) find ways to maintain the operating temperature performance of the Nd-Fe-B based PM without critical elements. The first scenario is unlikely in the near term because many significant large-scale research efforts, conducted since 2012, have yet to discover such new, powerful PM materials. While there have been some intriguing PM discoveries, many of these materials are far from commercial applications or even full lab demonstrations. There has also been considerable effort in new topologies for PM based motors that have been promising [6]. In fact, better integration between PM materials research and motor design is needed to foster advances in both arenas.

Most of the success has been in more efficient use of heavy REE, such as diffusing Dy only into the near surfaces of the Nd-Fe-B PMs that experiences the highest demagnetization fields [7]. Another promising route is to reduce the grain size (< 5 μm) of the Nd-Fe-B PMs to produce higher coercivity (H_{ci}) and operating temperature without heavy REE additions [8, 9]. The smaller grains are more resistant to field reversals and having more grains in a given volume hardens the overall magnet. However, reducing the grain size doesn't improve the slope of the temperature dependence of the coercivity, it simply shifts up the whole H_{ci} (T) curve. Our initial investigations on grain size effects on the properties of heavy REE free sintered PMs has shown that even modest reductions in the grain size can result in significant improvements in H_{ci} (Figure 1). However, this work has revealed that the mode of milling, their energy inputs and mechanism for commutating particles affects particle shape and size distribution. Also critical is powder handling since particle surfaces make up a much higher fraction of the volume. Special care in handling the powders is

required to keep the uncontrolled surface oxidation at a minimum.

To address this, Ames Laboratory has developed a Controlled Atmosphere Materials Processing System (CAMPS). CAMPS provides a solution for synthesis of high quality magnets in an environment that limits potential for oxidation and moisture contamination. It enables multiple complex materials synthesis operations to be performed in inert atmosphere. Within the same inert atmosphere, materials can be milled, magnetized, compacted and heat-treated. An optical microscope in the CAMPS allows for the imaging of particles during processing. One of the key enabling features of CAMPS is that the tools for the operations are in inert chambers while most of the control of the operations are performed outside of the chamber.

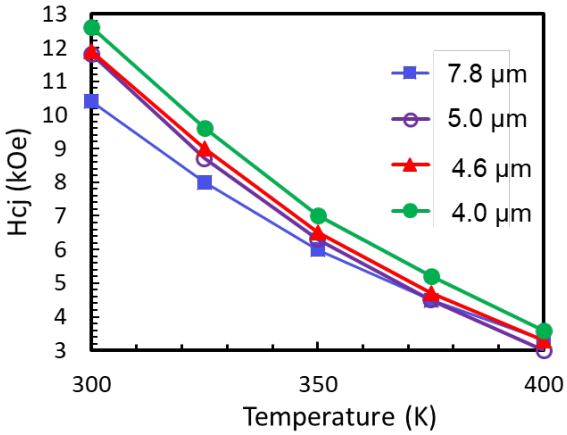

Figure 1. Effect of average grain size on the temperature dependence of the corecivity. The energy product also increased from 34.8 to 43.6 MGOe at room temperature with decreasing grain size.

The other challenge is to limit the grain growth during sintering of the superfine feedstock powder. We are investigating lower sintering temperatures, using excess REE as well as other external transient liquid phase to further reduce sintering temperature while achieving full magnet densification. Adding a grain boundary pinner may also be necessary to prevent grain growth. The extra effort in grain size reduction will be for naught if a fully dense; oxide free part that maintains the small grain size cannot be fabricated.

Non-rare earth magnets can be used for EV traction motor if the strict requirement of high power density and low cost can be met. One approach to mitigate the impact of weaker magnet on the motor density is to increase motor excitation frequency. However, this also creates other challenges. For example, at higher frequency, the hoop stress will be higher and eddy losses will be much higher in both soft and hard magnetic materials. We will present results on a recently completed project demonstrating that a 10 KW motor with power density of 1.2 KW/kg and 4.3 KW/L using MnBi PM. The motor run at 400 Hz. Its stator is made of 6.5%Si steel, which has 50% higher electrical resistivity comparing the common 3.2%Si steel. The motor maintained 90% efficiency when running at full power.

References

1) Critical Materials Strategy, U.S. DOE, http://energy.gov/sites/prod/files/edg/news/documents/criticalmaterialsstrategy.pdf, 2010
2) U.S. Geological Survey, 2020, Mineral commodity summaries 2020: U.S. Geological Survey, 200 p., https://doi.org/10.3133/mcs2020.
3) For instance see: metals-m@argusmedia.com
4) http://www.adamasintel.com/wp-content/uploads/2019/06/Adamas-Intelligence-Rare-Earths-Small-Market-Big-Necessity-Q2-2019.pdf
5) http://www.adamasintel.com/wp-content/uploads/2019/07/Adamas-Intelligence-Rare-Earths-Market-Issues-and-Outlook-Q2-2019.pdf
6) Swanke, J., Bobba, D., Jahns, T. M. & Sarlioglu, B. in 2019 IEEE Transportation Electrification Conference and Expo (ITEC). 1, DOI 10.1109/itec.2019.8790587.
7) Sepehri-Amin, H., Ohkubo, T. & Hono, K. Grain boundary structure and chemistry of Dy-diffusion processed Nd–Fe–B sintered magnets. J Appl Phys 107, 09A745, doi:10.1063/1.3351247 (2010).
8) Nothnagel P, Müller KH, Eckert D, Handstein A. The influence of particle size on the coercivity of sintered NdFeB magnets. Journal of Magnetism and Magnetic Materials. 1991 Oct 1; 101(1-3):379.
9) Sagawa, Masato. "Sintered NdFeB magnet and method for manufacturing the same." U.S. Patent No. 9,589,714. 7 Mar. 2017.

Enhancement of magnetic anisotropy of $L1_0$-FeNi nanoparticles and the related compounds for realization of rare-earth free magnet

Sho Goto[1], Eiji Watanabe[1], Yoshiaki Hayashi[1], Takahiro Nishio[1], Hiroaki Kura[1], Takashi Suemasu[2], Hideto Yanagihara[2], Eiji Kita[2], Takashi Honda[3], Keita Ito[4,5], Yusuke Shimada[4], Masahito Tsujikawa[5,6], Masaki Mizuguchi[4,5], Masafumi Shirai[5,6,7], Toyohiko Konno[4], Koki Takanashi[4,5,7]

[1] Advanced Research and Innovation Center, DENSO CORPORATION, Aichi, 470–0111, Japan.

[2] Department of Applied Physics, University of Tsukuba, Ibaraki, 305–8573, Japan.

[3] Institute of Materials Structure Science, High Energy Accelerator Research Organization, Ibaraki 305-0458, Japan

[4] Institute for Materials Research, Tohoku University, Sendai 980-8577, Japan

[5] Center for Spintronics Research Network, Tohoku University, Sendai 980-8577, Japan

[6] Research Institute of Electrical Communication, Tohoku University, Sendai 980-8577, Japan

[7] Center for Science and Innovation in Spintronics, Core Research Cluster, Tohoku University, Sendai 980-8577, Japan

In recent years, with the growing awareness of the environment, expectations for the development of high-performance motors for reducing power consumption are increasing. Especially in the automobile industry, the shift to electrified vehicles is progressing rapidly on a global scale, and the importance of high-performance motors is increasing year by year. General automobiles are equipped with more than 100 motors, including a drive main motor, and there is a demand for improved performance and cost reduction of motor products. The functions required of magnets vary depending on the intended use of the motor, such as high magnetization, high coercive force, heat resistance, and rust prevention. For products that are required high torque, such as drive main motors, strong magnets with high coercive force and high magnetization are required. In addition, heat resistance is also important because it is expected to be used under high load. On the other hand, water pumps, oil pumps, etc. are required to have rust prevention properties rather than magnetic performance. In future magnet development, not only the improvement of the maximum energy product $(BH)_{max}$ of the magnet but also the variety of functions will be important.

Meanwhile, the material we focused on was $L1_0$-FeNi. $L1_0$-FeNi is a material discovered in the 1960s , which is known to be present in iron meteorites in very small amounts.[1)] Although $L1_0$-FeNi does not contain rare earths, its uniaxial magnetic anisotropy energy (K_u) is 1.3×10^6 J/m^3 and its saturation magnetization is 1.6 T, which is expected to be comparable to neodymium magnets. In addition, the Curie temperature of $L1_0$FeNi is said to be 550 °C or higher, so it can be expected to be used at high temperatures. A lot of studies on $L1_0$-FeNi have been made to date, [1)-7)] but most of them were fundamental; the degree of order and/or the fraction of $L1_0$-phase were not enough.

Aiming at the practical application of $L1_0$-FeNi, we have developed the Nitrogen Insertion and Topotactic Extraction method (NITE) [8)] as a method that can stably synthesize high-quality $L1_0$-FeNi. A schematic diagram of the NITE method is shown in Fig. 1. The long-range order parameter (S) of $L1_0$-FeNi prepared by the NITE method was $S = 0.71$, and the coercive force was 142 kA / m. This coercive force is small for application as a magnet. The small coercive force seems to be caused by crystal grains are not magnetically isolated by sintering and Ku is low. In particular, improving K_u is important from the viewpoint of securing the potential of materials.

We are trying to improve K_u of $L1_0$-FeNi by two approaches. The first approach is to improve the S. In general, K_u of $L1_0$-type ordered alloy is said to increase in proportion to the square of S.[5),9)] In the NITE method, the ordered structure of $L1_0$-FeNi inherits the structure of the precursor FeNiN. Therefore, in order to obtain $L1_0$-FeNi with high S, it is important that Fe and Ni are completely ordered in the state of FeNiN. Therefore, in order to understand the ordered state of FeNiN, the arrangement of Fe, Ni, and N atoms was investigated using neutron diffraction. In conclusion, it was found that FeNiN is ordered by about 100% in Fe and Ni, and N atoms are in the Fe atomic plane. It was found that the denitriding process needs to be improved as the new issue to improve the S of $L1_0$-FeNi. Another approach to improving K_u is to increase tetragonality. $L1_0$-FeNi has a c / a value is almost unity showing contrast to other $L1_0$ type ordered alloys such

as FePt with 0.96 of c / a.[10] Theoretical studies have been conducted to improve K_u if the crystals can be distorted to change c / a. In this study, we propose ordered-FeNi-N_x (x = 0 to 1) in which an arbitrary amount of nitrogen is introduced into $L1_0$-FeNi as a means for changing c / a. According to the first principles calculations, $K_u = 1.61\times10^6$ J/m^3 was obtained for c / a = 1.025 at x = 0.25, and $K_u = 1.96\times10^6$ J/m^3 for c / a = 0.992 at x = 0.5, leading to larger K_u than that of $L1_0$-FeNi. It is considered that K_u is improved by the tetragonality of the crystal structure by N-doping. The ordered-FeNi-N_x was synthesized by topotactic nitriding of $L1_0$-FeNi. As a result, the nitride had two phases with x of 0.5 and 1.0, and the nitrogen content was not continuously controlled. For x = 0.5 the crystal structure as shown in Fig. 2 is expected. From the crystal structure analysis, the lattice constants were estimated to be a = 3.78Å, c = 3.73Å, and c / a = 0.988, and we have succeeded in distorting the crystal by introducing N as theoretically expected. However, the magnetic measurement gave the coercive force of ordered-FeNi-$N_{0.5}$ much smaller than that of $L1_0$-FeNi. The reason for the discrepancy with the calculation results is currently under investigation.

In order to put $L1_0$-FeNi into practical use as a magnet, we need to work on further improving S, making crystals tetragonality, and magnetically isolating crystal grains.

Acknowledgements

This paper is based on results obtained from the Future Pioneering Program “Development of magnetic material technology for high-efficiency motors” commissioned by the New Energy and Industrial Technology Development Organization (NEDO).

Reference

1) L. Néel et al., J. Appl. Phys., 35 (1964).
2) J. F. Albertsen, et al., Nature 273 (1978) 453.
3) P. Wasilewski et al., Earth Planet. Inter., **52** (1988) 150.
4) T. Kojima et al., Jpn. J. Appl. Phys., **51** (2012) 010204.
5) Y. Miura et al., J. Phys. Condens. Matter, **25** (2013) 106005.
6) T. Mohri, J. Mater. Sci., **50** (2015) 7705.
7) A. Makino et al., Sci. Rep. **5** (2015) 16627.
8) S. Goto et al., Sci. Rep. **7** (2017) 13216.
9) S. V. Komogortsev et al., Appl. Phys. Lett. **103** (2013) 152404.
10) J. Crangle et al., J. A. Philos. Mag. **38** (1983)1.

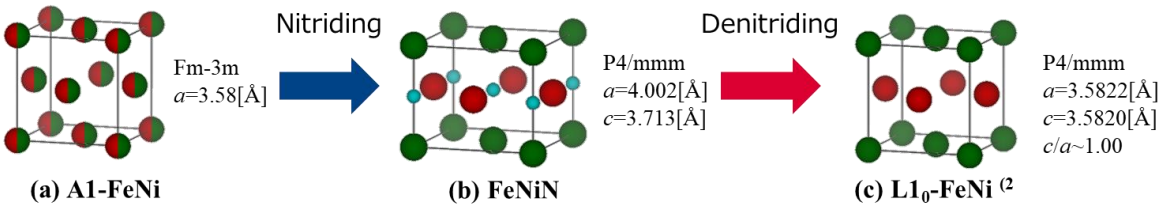

Fig.1 Conceptual diagram for fabrication path of ordered FeNi alloys by NITE method Models of crystal lattices for (a) A1-FeNi, (b) FeNiN, and (c) $L1_0$-FeNi are depicted with Fe (red), Ni (green), and N (light blue) atoms. Atoms identified by red and green indicate that Fe and Ni are randomly arranged according to the ratios of colored areas.

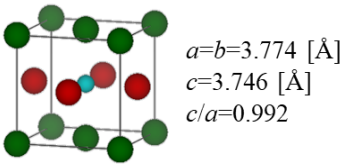

Fig.2 Crystal structure model of ordered-FeNi-$N_{0.5}$. This structure is expected to have a smaller c / a value than $L1_0$-FeNi.

Prospect of 1-12 based permanent magnets

~ Demonstration of high coercivity in thin films and current status of 1-12 bulk magnet~

[1]Y.K. Takahashi, [1]D. Ogawa, [1]H. Sepehri-Amin, [2]T. Shima, [1]T. Ohkubo, [1]S. Hirosawa, [1]K. Hono
([1]NIMS, [2]Tohoku Gakuin Univ.)

$SmFe_{12}$-based compound is one of the candidates for next generation permanent magnet due to its high saturation magnetization ($\mu_0 M_s$), high anisotropy (K) and high Curie temperature (T_c) [1]. Since $SmFe_{12}$-based compound is unstable at RT, the addition of the phase stabilizing element is necessary, which causes large reduction in magnetization. Recently, Kuno *et al.*[2] reported high $\mu_0 M_s$ by reducing Ti composition which is one of the phase stabilizing elements and substituting Fe and Sm with Co and Zr, respectively. Later, Hirayama *et al.* [3] prepared the single crystal $Sm(Fe_{0.8}Co_{0.2})_{12}$ film by sputtering and demonstrated high magnetic properties of $\mu_0 M_s$=1.78 T, H_a =12 T and T_c =859 K., which are superior to those of $Nd_2Fe_{14}B$. Even in the working temperature of the motor in electric vehicle (EV) or hybrid EV (HEV), these properties are higher than those of $Nd_2Fe_{14}B$. One drawback in $Sm(Fe_{0.8}Co_{0.2})_{12}$ compound is too low coercivity ($\mu_0 H_c$) for the permanent magnet application. In order to demonstrate the high $\mu_0 H_c$, we have controlled the microstructure by the diffusion process [4] and cosputtering of the nonmagnetic elements [5].

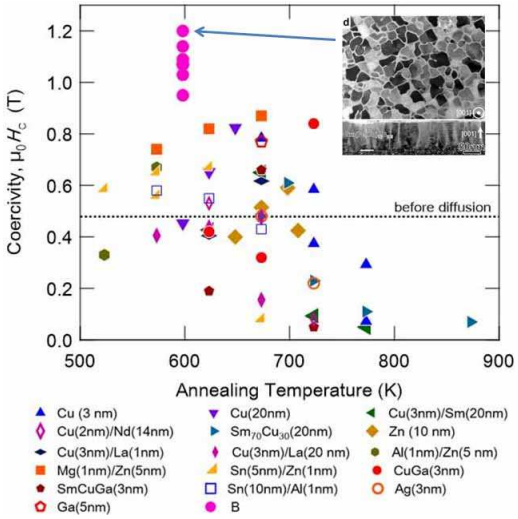

Fig. 1 Change of $\mu_0 H_c$ of the diffusion processed $Sm(Fe_{0.8}Co_{0.2})_{12}$ film as a function of annealing temperature. $\mu_0 H_c$ of the cosputtered $Sm(Fe_{0.8}Co_{0.2})_{12}$-B film is also shown.

Fig. 1 shows $\mu_0 H_c$ of the diffusion processed $Sm(Fe_{0.8}Co_{0.2})_{12}$ film as a function of annealing temperature. The optimum annealing temperature ranges from 623 K to 723 K. Cu, Cu-Ga, and Mg-Zn are the effective infiltration sources for igh $\mu_0 H_c$ corresponding to 0.78 T, 0.84 T, and 0.87 T, respectively. The microstructure of Cu-Ga diffused sample shows that the Cu and Ga are diffused into the grain boundary of $Sm(Fe_{0.8}Co_{0.2})_{12}$ grains. However, Cu and Ga do not form uniform intergranular phase. It could be the reason for marginal increase of $\mu_0 H_c$. B containing sample shows the highest $\mu_0 H_c$ of 1.2 T. As shown in the in-plane and cross-sectional TEM images of the inset, it forms well-separated nanogranular microstructure with about 40 nm diameter of $Sm(Fe_{0.8}Co_{0.2})_{12}$ grains perfectly enveloped by the B-rich amorphous grain boundary phase. Because of the magnetization and anisotropy difference between $Sm(Fe_{0.8}Co_{0.2})_{12}$ grains and grain boundary phase, the highest $\mu_0 H_c$ of 1.2T was achieved. Fig. 2 shows the temperature dependence of $\mu_0 H_c$ in the $Sm(Fe_{0.8}Co_{0.2})_{12}$ films with high $\mu_0 H_c$. Those in the commercial Nd-Fe-B magnets are shown for the comparison. $Sm(Fe_{0.8}Co_{0.2})_{12}$ films with high $\mu_0 H_c$ have small absolute value of temperature coefficient of coercivity (β ~ -0.2 %/K) due to the high T_c. These results indicate that $Sm(Fe_{0.8}Co_{0.2})_{12}$ could be a superior compound for permanent magnet application compared to $Nd_2Fe_{14}B$ magnet if optimum microstructure can be achieved in bulk with high $\mu_0 H_c$. In the talk, I would review current status of the investigation for 1-12 bulk magnet.

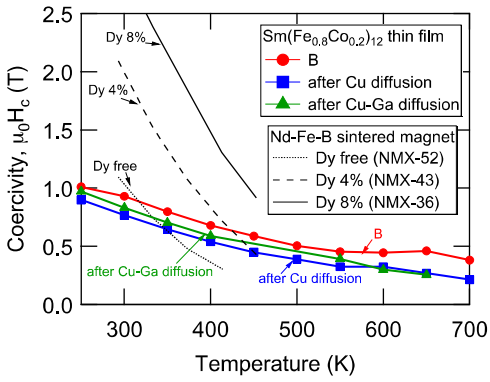

Fig. 2 Temperature dependence of $\mu_0 H_c$ in Nd-Fe-B magnets, $Sm(Fe_{0.8}Co_{0.2})_{12}$ film with Cu and Cu-Ga diffusion.

(1)K. Ohashi *et al.*, *IEEE Trans Magn*.**23**, 3101 (1987).(2)T. Kuno *et al.*, *AIP Adv.* **6** 025221 (2016). (3) Y. Hirayama *et al*, *Scr. Mater.***138**, 62 (2017). (4) D. Ogawa *et al*, Scr. Mater164, 140 (2019). (5) H. Sepehri-Amin *et al*, Acta Mater194, 337 (2020).

First-principles Study of Thermodynamic Stability in Multi-elements Alloying $(Sm,X)(Fe,Y)_{12}Z$ Compounds

Saengdeejing Arkapol, Chen Ying
(School of engineering, Tohoku University)

$SmFe_{12}$-based compounds have been considered one of the most promising candidates for the next generation high performance magnetic materials. $SmFe_{12}$-based compounds exhibit excellent intrinsic hard magnetic properties with lesser amount of rare earth elements compare to other hard magnetic materials, while synthesizing $SmFe_{12}$ compounds faces a big difficulty due to the thermodynamic stability of these compounds. Additional elements doping has been attempted to stabilize $SmFe_{12}$ compounds. Ti is currently one of the best elements to thermodynamically stabilize $SmFe_{12}$ compounds but it degrades the magnetic properties. Multi-element alloying approach is generally required to achieve the desired stability while minimized the degradation of the magnetic properties. In order to understand the effect of multi-elements on the stability and magnetic properties of $SmFe_{12}$-based compounds with multi-element alloying, systematical calculations of $(Sm,X)(Fe,Y)_{12}Z$ (X=Zr/Ce, Y=Co/V/Ti, Z=B) have been conducted.

The first-principles calculations become increasingly difficult due to the complexity of the structures. The supercell with larger number of atoms to represent the correct composition and random arrangement of atoms becomes inevitable. The Special Quasirandom Structure (SQS) model is adopted to imitate the random atomic configurations. The electronic structure and total energy at 0K are calculated by DFT, the contribution of the lattice vibration at finite temperature to the free energy is obtained from Debye-Grüneisen model[1].

Several SQS for multi-elements alloying in $(Sm,X)(Fe,Y)_{12}Z$ are generated. It is found that all structures are thermodynamically stable with respect to the referent state which is consists of ground state structures of component elements. Equation of state fitting is performed on each SQS to obtain parameters required for Debye-Grüneisen model to evaluate the vibrational free energy. Figure 1 shows the SQS model(a) and calculated free energy as a function of temperature in $Sm(Fe_{0.75}V_{0.25})_{11.5}Ti_{0.5}$ (b), as an example. Different contributions to the free energies are plotted separately to illustrate the magnitude of each contribution to the free energy. It is found that most of 3d transition elements seem to stabilize the $SmFe_{12}$ structure through the vibrational contribution to the free energy in single element doping ($SmFe_{11}Y$). Increasing the concentration of alloying elements beyond $SmFe_{11}Y$ tends to destabilize the structure at the lower temperature. The contributions to the stability of $SmFe_{12}$ compound from the configurational entropy is also important in some systems such as $Sm(Fe_{0.75}Co_{0.25})_{11}V_{0.5}Ti_{0.5}$. By carefully balancing between intrinsic formation energy at 0K, vibrational contribution and configurational entropy, it is possible to design the multi-element alloying $SmFe_{12}$ compound with optimum thermodynamic stability and magnetic properties.

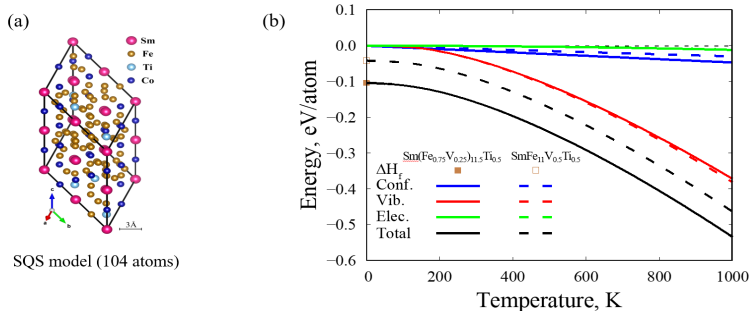

Figure 1: (a)The SQS model for random mixing of Sm $(Fe_{0.75}V_{0.25})_{11.5}Ti_{0.5}$. (b)Free energy at temperature up to 1000K and contributions of each physical effects in $Sm(Fe_{0.75}V_{0.25})_{11.5}Ti_{0.5}$ with comparison to $SmFe_{11}V_{0.5}Ti_{0.5}$.

Reference

1) Moruzzi V.L., et al. *Phys. Rev. B* 37 (1988) 790.

Chemical Synthesis of (Sm,Zr)(Fe,Co,Ti)$_{12}$ Magnetic Mesoscopic Particles

T. T. Trinh, R. Sato and T. Teranishi
(Institute for Chemical Research, Kyoto University)

Multielement (Sm,Zr)(Fe,Co,Ti)$_{12}$ ($ThMn_{12}$, *I*4/*mmm*) compounds have the potential to meet current demands for rare-earth-element-lean permanent magnets with ultra-large energy product and operating temperatures of 150–200 °C. However, their magnets with substantial coercivities have not been realized yet despite their impressively large magnetic anisotropy field and enormous research efforts. The following critical issues make it extremely challenging to practically realize their hard magnetic potential: unoptimized particle size and shape, especially in the mesoscopic scale; introduction of inappropriate intergranular boundary phases resulted from the simultaneous formation of equilibrium ferromagnetically soft phases (e.g., Fe, Co, FeCo) along with the typical (Sm,Zr)(Fe,Co,Ti)$_{12}$ phase; difficulty in fabricating anisotropic magnets using liquid-phase sintering due to relatively high melting temperature of the compounds. Herein we present our recent achievements in the advanced chemical synthesis of ultrafine (Sm,Zr)(Fe,Co,Ti)$_{12}$ mesoscopic particles with controllable grain-size and composition. As a result, their average size of *ca.*1 μm was obtained by thermodynamic control (Fig. 1A, B). Interestingly, we could simultaneously introduce a thin Sm surface (*ca.*2 nm) (Fig. 1A), which can serve as a non-magnetic intergranular boundary. Although the resultant particles exhibited relatively low remanence and coercivity, they were highly susceptible to magnetic-field alignment (Fig. 1C), promising a high potential for the fabrication of anisotropic magnets using a rapid low-temperature current sintering method. Synthetic prospects will move a step forward in the size control through kinetics to obtain their particle size in the range below 1 μm, where an ultra-large coercivity could be achieved.

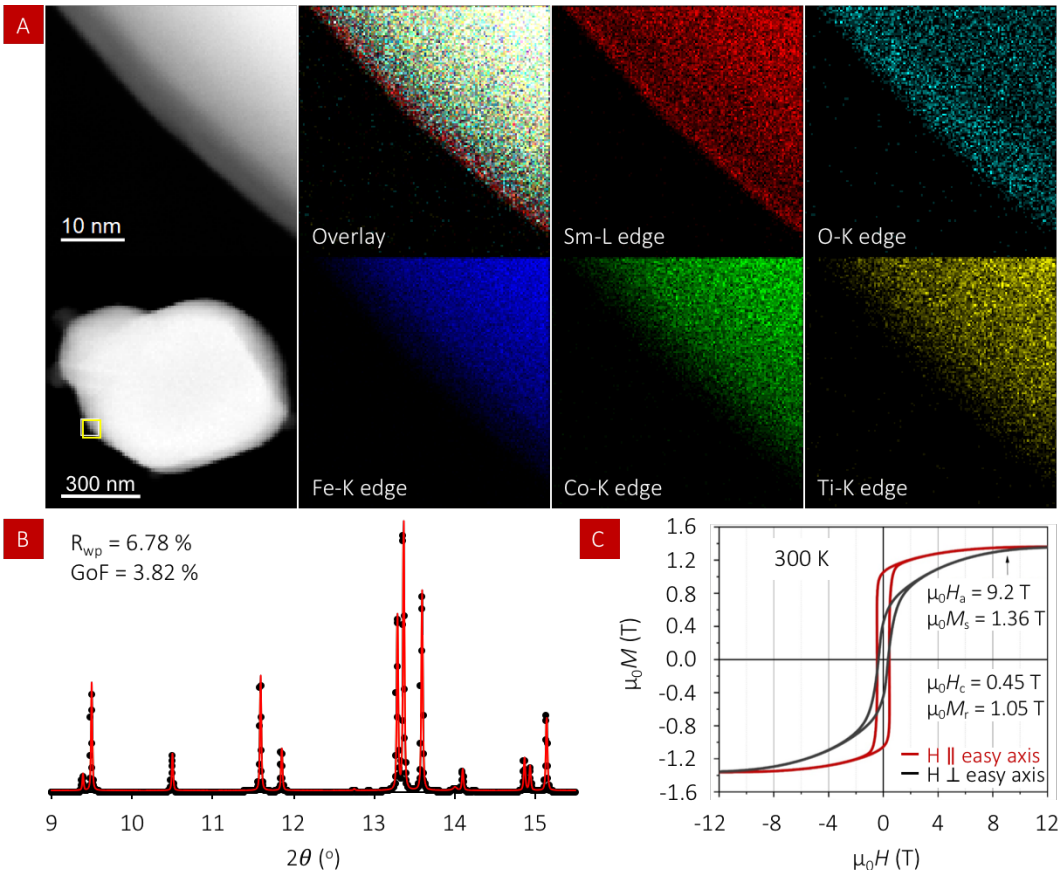

Fig. 1 Structural analysis and magnetic properties of chemically synthesized Sm(Fe$_{0.8}$Co$_{0.2}$)$_{11}$Ti@Sm core@shell mesoscopic particles: (A)HAADF and EDS elemental mapping image, (B) Rietveld refinement synchrotron XRD pattern, and (C) M–H curves.

Atomistic study of thermally-activated magnetization processes in rare earth permanent magnets

Seiji Miyashita[1,2], Masamichi Nishino[2,3], Yuta Toga[1,2], Taichi Hinokihara[1,2], Takashi Miyake[2,4], Hisazumi Akai[1,2], Satoshi Hirosawa[2], Akimasa Sakuma[5]

[1]Institute for Solid State Physics, The University of Tokyo, Kashiwa 277-8581, Japan
[2]ESICMM, National Institute for Materials Science (NIMS), Tsukuba, Ibaraki 305-0047, Japan
[3]International Center for Materials Nanoarchitectonics, NIMS, Tsukuba, Ibaraki 305-004, Japan
[4]CD-FMat, National Institute of Advanced Industrial Science and Technology (AIST), Tsukuba, Ibaraki 305-8568, Japan
[5]Department of Applied Physics, Tohoku University, Sendai 980-8579, Japan

For practical use of magnets, in particular at high temperatures, it is very important to study temperature dependence of magnetic properties [1,2]. We present our trials on this problem for the high-performance $Nd_2Fe_{14}B$ magnets (Fig.1). For this purpose, first we constructed an atomistic Hamiltonian to properly take into account the temperature [3]. With it, we calculated various thermodynamic quantities by methods of statistical physics, e.g., a constrained Monte Carlo method [3] and a stochastic LLG equation [4]. We confirmed that temperature dependences of the magnetization and anisotropy energies well reproduce the corresponding experimental results (Figs.2) [3]. Moreover, microscopic properties, e.g. the domain wall profiles [5], anisotropy of the exchange coupling constant reflecting the crystal structure [6], and also dynamical properties, e.g., the spectrum of FMR (ferromagnetic resonance) [7] were also studied. As a merit of the atomistic model, we can find atom-specific ordering properties [3].

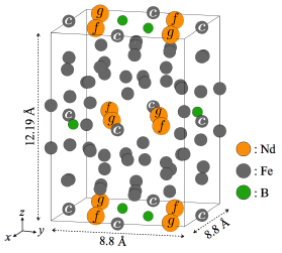

Fig.1 Unit cell of $Nd_2Fe_{14}B$

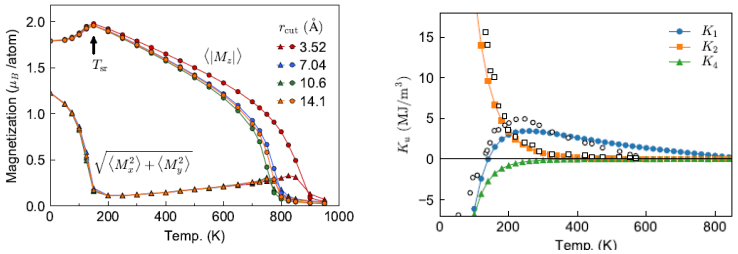

Fig.2 Temperature dependence of magnetization and anisotropy constants [3].

The most important property of magnets is the coercivity. However, in contrast to the above-mentioned thermodynamic quantities, we do not have theoretical formula for the coercivity, and thus so far only little study has been done on quantitative estimation of the coercivity at finite temperatures. We studied this problem in nano-size grains by a method using the free-energy landscape obtained by Wang-Landau method [8], and also by a direct dynamical simulation of the stochastic LLG equation [9]. There, the

strength of magnetic field at which the relaxation time of the magnetization reversal is 1second (a definition of coercivity) and its temperature dependence are obtained.

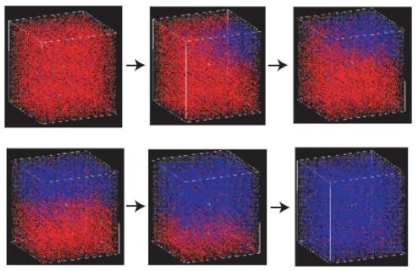

Fig.3 Magnetization reversal in a nano grain [9]

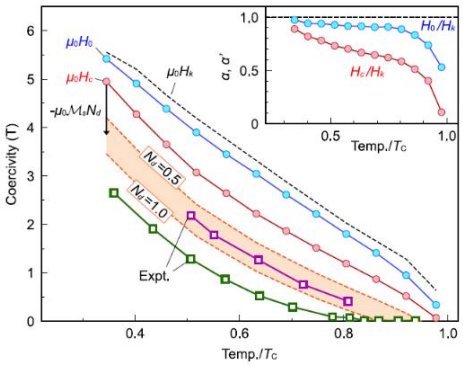

Fig. 4 Temperature dependences of coercivities [8]

It was found that the coercivity at a high temperature (about half of the critical temperature) is around 3T which is the theoretical maximum value although it is significantly reduced from the one at zero temperature. For larger grains, the dipole-dipole interaction plays a role [10] and the multidomain magnetic structure appears [11]. We also discuss a mechanism of coercivity in such cases. Real magnets consist of hard magnet ($Nd_2Fe_{14}B$) grains each of which are covered by grain boundary material. Thus, it is important to study how the boundary phases affect the coercivity [12], which is also presented. Finally, ensemble effects of gains on the coercivity are also reported from a viewpoint of the first-order reversal curves (FORC).

[1] S. Hirosawa, M. Nishino, S. Miyashita, Adv. Nat. Sci.: Nanosci. Nanotechnol. **8**, 013002 (2017).

[2] S. Miyashita, M. Nishino, Y. Toga, T. Hinokihara, T. Miyake, S. Hirosawa and A. Sakuma, Scripta Materialia, **154**,259 (2018).

[3] Y. Toga, M. Matsumoto, S. Miyashita, H. Akai, S. Doi, T. Miyake, and A. Sakuma: Phys. Rev. B 94, 174433 (2016). & Phys. Rev. B **94**, 219901 (2016).

[4] M. Nishino and S. Miyashita, Phys. Rev. B**91**, 134411(1-13) (2015).

[5] M. Nishino, Y. Toga, S. M., H. Akai, A. Sakuma, and S. Hirosawa, Phys. Rev. B **95**, 094429 (2017).

[6] Y. Toga, M. Nishino, S. Miyashita, T. Miyake, and A. Sakuma, Phys. Rev. B **98**, 054418 (2018) .

[7] M. Nishino, S. Miyashita: Phys. Rev. B **100**, 020403(R) (2019).

[8] Y. Toga, S. Miyashita, A. Sakuma and T. Miyake, npj Computational Materials **6**, 67 (2020).

[9] M. Nishino, I. E. Uysal, T. Hinokihara, and S. Miyashita, Phys. Rev. B **102**, 020413(R) (2020).

[10] T. Hinokihara, M. Nishino, Y. Toga, and S. Miyashita, Phys. Rev. B97, 104427 (2018).

[11] T. Hinokihara and S. Miyashita, arXive:2009.11574

[12] I. E. Uysal, M. Nishino, S. Miyashita, Phys. Rev. B **101**,094421 (2020).

[13] M. Nishino, I. E. Uysal , T. Hinokihara S. Miyashita, arXive:2009.08572

Nd-Fe-B 磁石の保磁力に対する表面 Nd の磁気異方性の効果

西野正理[1]、Ismail Enes Uysal[1]、宮下精二[2,1]
（[1]物材機構、[2]東大物性研）

The effect of the surface magnetic anisotropy of Nd atoms on the coercivity in Nd-Fe-B magnets

Masamichi Nishino[1], Ismail Enes Uysal[1], and Seiji Miyashita[2,1]
([1]NIMS, [2]ISSP, Univ. of Tokyo)

イントロダクション

ネオジム磁石 N-Fe-B は高い保磁力を持ち、モーターや発電機などに利用されている。新規磁石材料設計には保磁力の機構解明が重要であるが、依然として未解明の部分が多い[1]。保磁力機構の微視的なスケールからの解明には、原子論に基づくモデル化とそのダイナミクスの解析が必要である。我々は、連続体モデルによるマイクロマグネティクス計算とは異なる方法論、すなわち、結晶格子を反映した原子論的スピンモデルを用いた方法論によるネオジム磁石の磁化反転解析を行ってきた[2]。保磁力制御のためには、磁気グレインの表面、界面の性質を知ることが重要である[1,3]。第一原理計算の研究において、(001)表面の Nd 原子の異方性はバルクにおける c 軸の容易軸とは異なり、 c 面が容易面となることで保磁力の低下の原因となり得るという報告がなされた[4]。我々は、表面の Nd 原子の磁気異方性に注目して、ゼロ温度と有限温度において、表面の異方性が保磁力にどのような影響を与えるかについて調べた[5]。

磁化反転における表面の効果

磁化ダイナミクスを記述する基礎方程式である Landau-Lifshitz-Gilbert(LLG)方程式に熱揺らぎの効果を取り込んだ方法論（Stochastic LLG 法[2]）をこの系に適用して解析を行った。原子論的モデルのミクロなパラメータは、主として第一原理計から見積もった値を用いている。図 1 のように(001)面の表面 Nd 層の n 層目までの Nd 原子に対する異方性を修飾して、その効果が反転磁場に与える効果を調べた。表面 Nd 原子の異方性の修飾の仕方として、(1) 磁気異方性が無い、(2) 容易面を持つ、(3)強化した容易軸異方性を持つ、それぞの場合について調べた。ゼロ温度では表面一層(n=1)のみ修飾しても反転磁場は大きく変化するが、室温付近では殆ど効かず、効果が現れるには数層の修飾が必要であることが分かった。同様に(100)面における表面効果についても調べ、比較した。本公演では、3 つの修飾の仕方に対して、表面の種類、温度、修飾層の深さといった因子が保磁力に及ぼす影響について議論する。

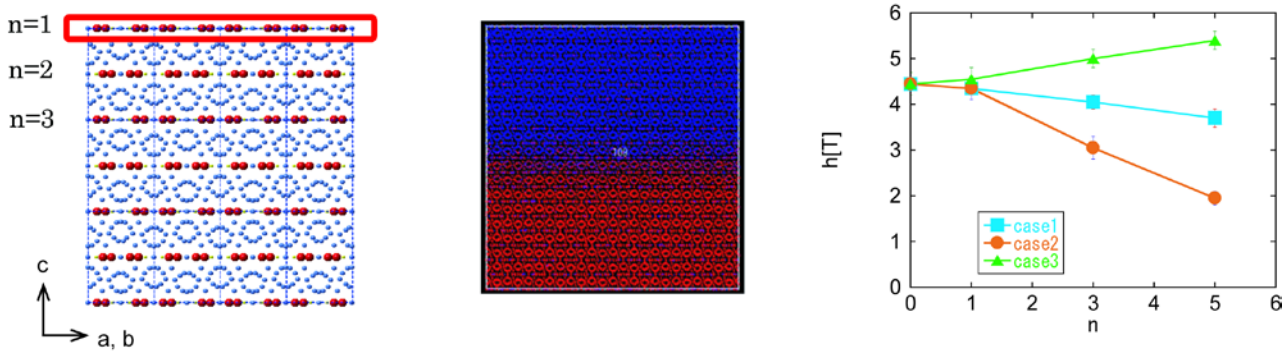

図1（左）(001)面におけるnの定義、（中）磁化反転の様子、（右）室温付近でのnに対する保磁力の変化。

参考文献

1) S. Hirosawa, M. Nishino and S. Miyashita, Adv. Nat. Sci.: Nanosci. Nanotechnol. 8, 013002 (2017).
2) M. Nishino, I. E. Uysal, T. Hinokihara, and S. Miyashita, Phys. Rev. B 102, 020413(R) (2020).
3) I. E. Uysal, M. Nishino, and S. Miyashita, Phys. Rev. B 101, 094421 (2020).
4) H. Moriya, H. Tsuchiura, and A. Sakuma, J. Appl. Phys. 105, 07A740 (2009).
5) M. Nishino, I. E. Uysal, and S. Miyashita, submitted. arXiv:2009.08572.

Observation of the demagnetization process of HDDR Nd-Fe-B sintered magnets by soft X-ray magnetic circular dichroism microscopy

A. Martin-Cid[1,2], T. Kawahara[3], S. Kobayashi[1,2], K. Toyoki[1,2], D. Billington[1,2], Y. Kotani[1], H. Kubo[3], Y. Une[3], T. Iriyama[3], M. Sagawa[3], T. Nakamura[1,2,4]

[1] Japan Synchrotron Radiation Research Institute (JASRI), 1-1-1 Kouto, Sayo 679-5198, Japan

[2] Elements Strategy Initiative Center for Magnetic Materials (ESICMM), National Institute for Materials Science, Tsukuba 305-0047, Japan

[3] Daido corporate research and development center, Daido steel Co., Ltd., 2-30 Daido-cho, Minami-ku, Nagoya 457-8545, Japan

[4] International Center for Synchrotron Radiation Innovation Smart, Tohoku University, Sendai 980-8577, Japan

Nd-Fe-B based magnets have dominated the high-performance permanent magnet market since their development in 1984. Among other applications, wind turbines and motors for electric-powered cars have experienced rapid growth due to the necessity to reduce the dependence on fossil fuels. Magnets used in these applications have to sustain high demagnetization fields under temperatures up to 200 °C, and so, as the temperature coefficient of coercivity of Nd-Fe-B magnets is large, a high coercivity ($\mu_0 H_c$ ~ 3.0 T) at room temperature (RT) is needed. As Nd-Fe-B sintered magnets present a relatively low coercivity ($\mu_0 H_c$ ~ 1.2 T) at RT, partial substitution of Nd with heavy rare earth (HRE) elements such as Dy or Tb is commonly used to improve the coercivity and thermal stability. In the attempt to reduce the use of the very scarce HRE, efforts are being made to improve the coercivity of HRE-free Nd-Fe-B sintered magnets by tuning the microstructure reducing the grain size of the main $Nd_2Fe_{14}B$ phase and improving the grain boundary phase of the sintered magnet. To obtain grain sizes below 1 μm, the hydrogenation-disproportionation-desorption-recombination (HDDR) and hydrogen decrepitation processes have been explored. Recently, Xu *et al*. [1] reported an unexpectedly low coercivity, of just 1.3 T, in sintered magnets with ultrafine grain sizes obtained by HDDR and the pressless sintering process (PLP) compared to those made from He jet-milling and PLP, with a coercivity of 2.14 T, while both had a similar particle size of ~1 μm. They found that HDDR processed PLP magnets presented a thinner grain boundary together with a lower concentration of non-magnetic elements in the grain boundary, which would promote the propagation of the reversal magnetic domains, and thus, reduce the coercivity.

To gain a deeper insight into the reason for the diminished coercivity on HDDR processed PLP magnets, in this work, we have analyzed the evolution of the magnetic domains on the fractured surface of four types of Nd-Fe-B-based magnets with different sizes of grains by soft X-ray magnetic circular dichroism (XMCD) microscopy. These include a hot deformed magnet with plate-like grains of ~0.37 μm with a thickness of ~100 nm in the c-axis direction, and three PLP magnets obtained from a N_2 jet-milled powder (~3 μm), a He jet-milled powder (~1 μm), and a HDDR powder (~0.8 μm), which is made by both HDDR and He jet-milling. The XMCD microscopy showed that, while the 3μm, the 1μm, and the hot deformed magnet demagnetization processes were mainly driven by nucleation and propagation of the reversal domains with a preference for the domain propagation in the hot deformed magnet, in the HDDR processed magnet, the nucleation of magnetic reversal domains dominates throughout the whole demagnetization process. Moreover, the nucleation field for the HDDR processed magnet is greatly reduced compared to the other magnets studied.

References

1) X.D. Xu *et al*., Acta Mater. 151 (2018) 293–300.

Hysteresis design of magnetic materials for efficient energy conversion

Oliver Gutfleisch

Material Science, Technical University Darmstadt, D-64287 Darmstadt, Germany

Abstract

Magnets are key components of energy-related technologies, such as direct drive wind turbines and e-mobility. They are also important in robotics and automatisation, sensors, actuators, and information technology. The magnetocaloric effect (MCE) is of strong interest for new and disruptive solid state-based refrigeration. Magnetic hysteresis – and its inherent energy product - characterises the performance of all magnetic materials. Despite considerable progress in the modelling, characterisation and synthesis of magnetic materials, hysteresis is a long-studied phenomenon that is still far from being completely understood. Discrepancies between intrinsic and extrinsic magnetic properties remain an open challenge and magnets do not operate yet at their physical limits. The design of hysteresis for the magnets for the above applications requires an expanded detailed knowledge on different length scales. Ultimately, new strategies for effective magnetic hardening mechanisms of permanent magnets resisting high external magnetic fields and temperatures and for strong thermomagnetic responses in low fields of magnetocaloric materials are needed.
In this context, I will introduce our newly established DFG Cooperate Research Center 270 Hommage Hysteresis Design of Magnetic Materials for Efficient Energy Conversion https://www.tu-darmstadt.de/sfb270.

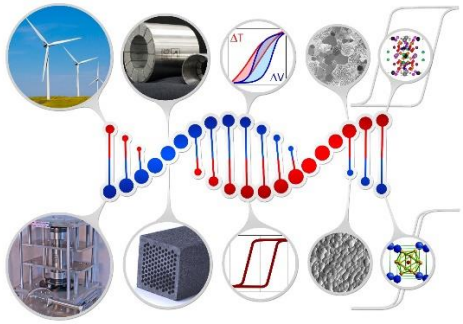

©*FunctionalMaterials*

[1] O. Gutfleisch, M. A. Willard, E. Brück, C. H. Chen, S. G. Sankar, and J. P. Liu, Magnetic materials and devices for the 21st century: stronger, lighter, and more energy efficient. Adv. Mater. 23 (2011) 82.
[2] K.P. Skokov and O. Gutfleisch, Heavy rare earth free, free rare earth and rare earth free magnets - vision and reality, Scripta Materialia View Point Set, 154 (2018) 289-294.
[3] T. Gottschall, A. Gracia-Condal, M. Fries, A. Taubel, L. Pfeuffer, L. Manosa, A. Planes, K.P. Skokov, O. Gutfleisch, A multicaloric cooling cycle that exploits thermal hysteresis, Nature Materials (2018).
[4] M. Duerrschnabel, M. Yi, K. Uestuener, M. Liesegang, M. Katter, H.-J. Kleebe, B. Xu, O. Gutfleisch, L. Molina-Luna, Atomic structure and domain wall pinning in samarium -cobalt based permanent magnets, Nature Communications 8:54 (2017).
[5] J. Liu, T. Gottschall, K.P. Skokov, J.D. Moore, O. Gutfleisch, Giant magnetocaloric effect driven by structural transition, Nature Mat. 11 (2012) 620.
[6] O. Gutfleisch, T. Gottschall, M. Fries, D. Benke, I. Radulov, K. P. Skokov, H. Wende, M. Gruner, M. Acet, P. Entel and M. Farle, Mastering hysteresis in magnetocaloric materials, Phil. Trans. R. Soc. A 374 (2016) 20150308.

Visualization of the magnetization reversal processes in He jet-milled Nd-Fe-B sintered magnet by X-ray magnetic tomography

M Suzuki[1], M. Takeuchi[2], S. Kobayashi[1,3], R. Haga[2], Y. Kotani[1], T. Nakamura[1,3,4], N. Kikuchi[2], T. Sasaki[3,5], T. Ohkubo[3,5], Y. Une[6], and S. Okamoto[2,3]
[1]Japan Synchrotron Radiation Research Institute, 1-1-1 Kouto, Sayo, 679-5198, Japan.
[2]IMRAM Tohoku University, Sendai 980-8577, Japan
[3]Elements Strategy Initiative Center for Magnetic Materials, NIMS, Tsukuba 305-0047, Japan.
[4]International Center for Synchrotron Radiation Innovation Smart, Tohoku University, Sendai 980-8577, Japan
[5]Research Center for Magnetic and Spintronics Materials, NIMS, Tsukuba 305-0047, Japan.
[6]Daido Corporate Research and Development Center, Steel Co., Ltd., Nagoya 457-8545, Japan

Introduction

The magnetic properties of Nd-Fe-B sintered magnets are closely related to the microstructure. To unveil the mechanism of the high coercivity emerged, the nucleation and evolution processes of reversed magnetic domains need to be clarified concerning the microstructure of a sintered magnet. Magnetic domain observation under an external magnetic field has so far been performed using Kerr microscopy and soft-X-ray scanning XMCD microscopy [1-4]. However, these existing techniques are limited to observe the domain structure on the surface of the sample, and it was not possible to investigate the magnetization reversal process inside bulk magnets. In this study, we used a recently developed hard X-ray magnetic tomography technique [5, 6] to directly observe the internal magnetic domain structure of Nd-Fe-B sintered magnets in a three-dimensional (3D) manner.

Experiment

Anisotropic Nd-Fe-B sintered magnet with an averaged particle diameter of 1 μm was prepared by the He-jet mill and pressless process [7]. A bulk specimen (remanent magnetization 1.5 T and coercivity 1.4 T) was micro-fabricated into a square column of 20×20×57 μm^3 by a focused ion beam (FIB) method. A first order reversal curve (FORC) measurement was performed for another cutting sample with the same aspect ratio and larger dimensions, and it was confirmed that the FIB process has given little damage and the magnetic properties of the sample were almost unchanged. The hard X-ray magnetic microtomography experiment at the Nd L_2 edge (6.725 keV) was carried out at BL39XU of SPring-8 [5, 6]. The application of magnetic fields to the sample was performed off-line, and the magnetic domain structure of the remanent magnetization state at zero fields was observed by the X-ray tomography measurements.

Results

The formation and reversal process of the magnetic domains inside the bulk Nd-Fe-B sample was successfully observed in 3D. The widths of magnetic domains are comparable to the particle diameter, suggesting that the magnetization reversal of each particle has been visualized. Some inner grains are found to reverse independently. Thus, the nucleation points of magnetization reversal are directly demonstrated. In this talk, the correlation between the sintered microstructure and the magnetic domain structure will be discussed.

Part of this work is supported by ESICMM under the outsourcing project of MEXT (JPMXP0112101004).

[1] M. Suzuki *et al*., Acta Mater. **106**, 155 (2016). [2] Y. Kotani *et al*., J. Synchrotron Rad. **25**, 1444 (2018). [3] D. Billington *et al*., Phys. Rev. Mater. **2**, 104413 (2018). [4] S. Okamoto *et al*., Acta Mater. **178**, 90 (2019). [5] M. Suzuki *et al*., Appl. Phys. Express **11**, 036601 (2018). [6] M. Suzuki *et al*., Synchrotron Rad. News **33**, 4 (2020). [7] Y. Une *et al*., J. Jpn Inst. Met. **76**, 12 (2012).

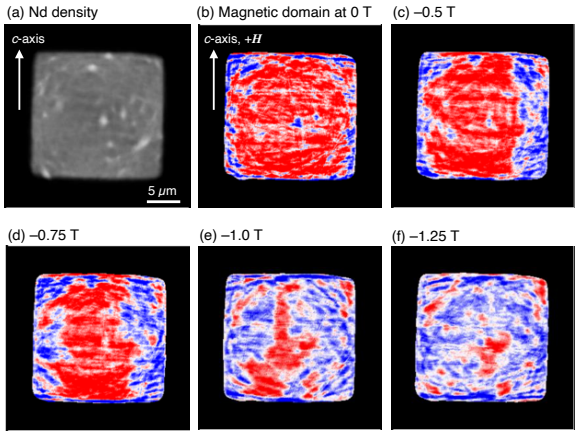

Fig. 1 Tomographic reconstructions of He-jet milled Nd-Fe-B sintered magnet. Cross sections of a square column sample at a plane parallel to the c-axis are shown.

Spins in Low-dimensional Materials Systems: Transport, Gate-control and Conversion

Masashi Shiraishi
(Department of Electronic Science and Engineering, Kyoto University, Japan)

Transport, control and conversion of spins in condensed matters have been pivotal concepts in spintronics. Spin transport is the most fundamental concept to realize spin-dependent phenomena, spin control mainly by gating enables information switching using a spin degree of freedom, and spin conversion allows detection of spins, a dissipative physical quantity. Whilst bulk metallic and semiconducting systems have been to date major material stages to realize the aforementioned concepts, low-dimensional materials systems such as atomically-flat two-dimensional materials [1-3], two-dimensional electron gases formed at an interface of a heterostructure [4,5], topologically-protected Dirac surface states in topological insulators [6,7] and ultrathin films [8] are becoming attractive materials stages to pursue novel spintronic concepts and phenomena. I will introduce the attractiveness of these new materials systems, cover an overview of the central achievements, and focus on recent investigation to pioneer novel spintronic physics in the low-dimensional materials systems.

Reference

1) B. Raes, S.O. Valenzuela et al., “Determination of the spin-lifetime anisotropy in graphene using oblique spin precession”, *Nature Commun.* 7, 11444 (2016).
2) S. Dushenko, M. Shiraishi et al., “Gate-tunable spin-charge conversion and the role of spin-orbit interaction in graphene”, *Phys. Rev. Lett.* 116, 166102 (2016).
3) A.W. Cummings, S. Roche et al., “Giant spin lifetime anisotropy in graphene induced by proximity effects”, *Phys. Rev. Lett.* 119, 206601 (2017).
4) R. Ohshima, M. Shiraishi et al., “Strong evidence for d-electron spin transport at room temperature at a $LaAlO_3/SrTiO_3$ interface”, *Nature Mater.* 16, 609 (2017).
5) E. Lesne, M. Bibes et al., “Highly efficient and tunable spin-to-charge conversion through Rashba coupling at oxide interface”, *Nature Mater.* 15, 1261 (2016).
6) Y. Shiomi, E. Saitoh et al., Spin-electricity conversion induced by spin injection into topological insulators”, *Phys. Rev. Lett.* 113, 196601 (2014).
7) Yuichiro Ando, M. Shiraishi et al., “Electrical detection of the spin polarization due to charge flow in the surface state of the topological insulator $Bi_{1.5}Sb_{0.5}Te_{1.7}Se_{1.3}$”, *Nano Lett.* 14, 6226 (2014).
8) S. Dushenko, M. Shiraishi et al., “Tunable inverse spin Hall effect in nanometer-thick platinum films by ionic gating”, Nature Commun. 9, 3118 (2018).

Strong-coupling phenomena in spintronics

Gerrit E.W. Bauer
AIMR and IMR, Tohoku University, Sendai, Japan

Traditional spintronic devices control the magnetic order digitally. Magnetic and electric fields, charge, spin, and heat currents, sound, microwaves, light, etc. can write a bit by switching the magnetization of a memory element between the “up” to “down” states. However, new computational classical and quantum architectures require analogue control over the magnetic texture. Ideally, the dynamic magnetization is manipulated coherently to point into any direction on the Bloch sphere, which requires control parameters that strongly couple to the magnetic order, i.e. an interaction strength that exceeds the lifetime broadening. Since magnetic dipoles interact only weakly with the environment, the strong-coupling regime of spintronics can be reached with high-quality materials and devices only.
The material of choice to study the physics and applications of strong coupling is yttrium iron garnet (YIG), an electrically insulating ferrimagnet with a Curie transition far above room temperature. Its record magnetic, acoustic and optical quality led already to the discovery of entirely new phenomena, such as the spin Seebeck effect, which raise the hope for new applications in a sustainable future electronics. Due to a decade of a global research effort, we now quantitatively understand much of YIG’s basic physics, such as the temperature-dependent spin dynamics and the interaction of the magnetic order with photons and phonons.
I will present a selection of our recent progress in the physics of YIG and our search for evidence for strong coupling in YIG devices.

Probabilistic Computing with Stochastic Magnetic Tunnel Junctions

Kerem Camsari[1,7], William A. Borders[2], Ahmed Z. Pervaiz[1], Shunsuke Fukami[2-5], Supriyo Datta[1] and Hideo Ohno[2-6]

[1]School of Electrical and Computer Engineering, Purdue University, USA,
[2]Laboratory for Nanoelectronics and Spintronics, Research Institute of Electrical Communication, Tohoku University, Japan
[3]Center for Spintronics Research Network, Tohoku University, Japan
[4]Center for Innovative Integrated Electronic Systems, Tohoku University, Japan
[5]Center for Science and Innovation in Spintronics, Tohoku University, Japan
[6]WPI-Advanced Institute for Materials Research, Tohoku University, Japan
[7]Department of Electrical and Computer Engineering, University of California, Santa Barbara, USA

Digital computing is based on deterministic bits that represent 0 or 1, with stable charges on a capacitor or ferromagnets with a stable magnetic orientation. Quantum computing on the other hand is based on q-bits that represent superpositions of 0 and 1, with coherent quantities such as a single spin or the phase of a superconducting junction. Here, we draw attention to something in between, namely, a probabilistic bit or a p-bit that fluctuates between 0 and 1 that can be represented by unstable entities such as stochastic nanomagnets [1-2].

While probabilistic bits are not substitutes for *coherent* quantum bits, many applications envisioned for Noisy Intermediate Scale Quantum (NISQ) devices are shared by p-bits. Examples include hardware accelerators for combinatorial optimization and sampling problems as well as inference and learning for machine learning applications. Interestingly, a class of quantum algorithms that are used by D-Wave's quantum annealers can be represented by p-bit networks as long as the encoded system belongs to a special subclass of quantum systems that are called "stoquastic". In the absence of extreme limitations brought on by the cryogenic operation to achieve phase coherence and entanglement in quantum computers, probabilistic networks could represent more complicated stoquastic problems with fewer number of p-bits due to the flexibility of their interconnections.

Naturally, probabilistic *emulators* can be built by conventional digital computers as well. As such, it is natural to ask why dedicated hardware for probabilistic computers would be needed. Our estimates indicate that pseudorandom generators implemented in straightforward digital CMOS requires more than 100X more area compared to a mixed-signal p-bit implementation from a slightly modified 1T/1MTJ cell of the commercial STT-MRAM technology. A much lower cell area results in both better *energy-efficiency* as well as *better scaling* to build larger p-bit networks.

Recently, in a tabletop experiment [1], we demonstrated that a network of 8 p-bits that make use of such stochastic MTJs with unstable free layers can be used to solve classical optimization problems in hardware. Fig. 1a shows the 1T/1MTJ building block (p-bit) that uses the stochastic MTJs developed by the Fukami / Ohno laboratory of Tohoku University. An essential feature of this design comes from its *asynchronous* nature, namely, that there is no global clock that synchronizes the dynamical evolution of the system, rather, each p-bit is free to make an update by considering the input it receives from its neighbors. An asynchronous design that satisfies this requirement can achieve a very large number of flips per second due to the possibility of designing *massively parallel* STT-MRAM chips with more than a million 1T/1MTJ cells that operate independently.

Reference
1) Borders et al., "Integer Factorization using Stochastic Magnetic Tunnel Junctions," Nature 573, 390 (2019).
2) Camsari et al., "p-bits for Probabilistic Spin Logic", Applied Physics Reviews, 6, 1, 2019.

Logic operation using electron spins in silicon

Yuichiro Ando and Masashi Shiraishi

(Kyoto University)

Logic gates using electron spins in silicon are expected to realize beyond complementary metal-oxide-semiconductor (CMOS) architectures with a superior switching energy, a high logic density, and a nonvolatile function. Here we focus on the semiconductor-based universal magnetologic gate (MLG) where the operand of logic operation is the magnetization direction [1]. The MLG consists of five ferromagnetic (FM) electrodes with parallel easy magnetization axes (Fig. 1(a)). The two collinear easy axes, $+y$ and $-y$, are defined as the binary states "1" and "0", respectively. The two outmost FM electrodes are input terminals and the center electrode is the output terminal. The other electrodes are configuration terminals that define the gate operation such as NAND or OR. By applying charge currents, spin accumulation is generated in the semiconductor channel, whose amplitude beneath the output electrode is represented by NAND or OR. Any binary logic operation can be realized by using a finite number of MLGs. Furthermore, the reconfigurable logic gates at a clock frequency provides flexibility in logic circuit design. An MLG consists of two exclusive or (XOR) gates. Therefore, logic operation of one XOR gate using three ferromagnetic electrodes (Fig. 1(b)) is a fundamental technique to realize MLG operation.

Here we present room temperature operation of a spin exclusive or (XOR) gate in lateral spin valve devices with nondegenerate silicon (Si) channels [2, 3]. The device for the spin XOR gate consists of three iron (Fe)/cobalt (Co)/magnesium oxide (MgO) electrodes. The spin drift effect was controlled by a lateral electric field in the Si channel to adjust the spin accumulation voltages detected by FM-M under two different parallel configurations of FM-A and FM-B, corresponding to (1, 1) and (0, 0), so that they exhibit the same value. As a result, the spin accumulation voltage detected by FM-M exhibited three different voltages, represented by an XOR gate in MLG as shown in Fig. 1(c). The one-dimensional spin drift-diffusion model clearly explained the obtained XOR behavior. Charge current detection of the spin XOR gate was also demonstrated. The detected charge current was 1.67 nA. Furthermore, gate voltage modulation of the spin XOR gate was also demonstrated, which enables operation of multiple MLG devices.

In the presentation, we will also report recent progress of the spin logic operation using spins in silicon.

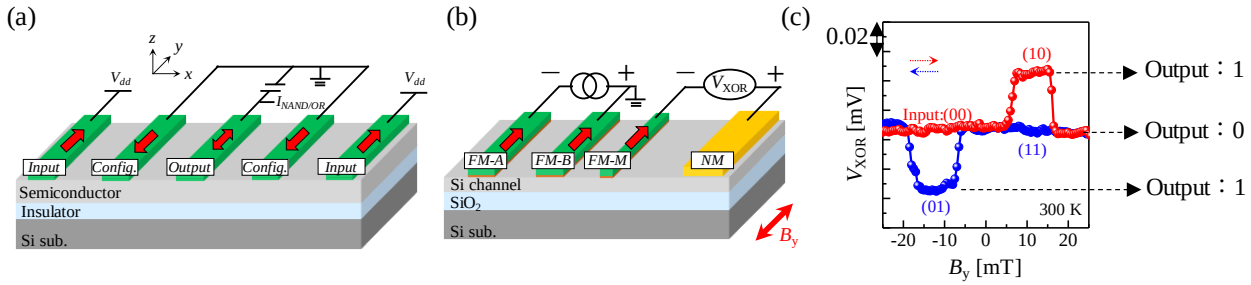

Figure 1 (a) Schematic illustration of the semiconductor-based MLG device proposed by Dery et al. [1]. (b) Schematic illustration of the silicon-based multiterminal lateral spin valves for the XOR operation. (c) A typical V_{XOR}-B_y curve in the XOR operation.

Reference

1) H. Dery, P. Dalal, Ł. Cywiński, and L. J. Sham, Nature **447**, 573 (2007).
2) R. Ishihara, Y. Ando, S. Lee, R. Ohshima, M. Goto, S. Miwa, Y. Suzuki, H. Koike and M. Shiraishi, Physical Review Applied **13**, 044010(2020).
3) R. Ishihara, S. Lee, Y. Ando, R. Ohshima, M. Goto, S. Miwa, Y. Suzuki, H. Koike and M. Shiraishi, AIP Advances **9**, 125326(2019).

Reservoir computing using dynamics of magnetic skyrmions

Tomoyuki Yokouchi
RIKEN Center for Emergent Matter Science (CEMS), Wako 351-0198, Japan.
Department of Basic Science, The University of Tokyo, Komaba, Tokyo 153-8902, Japan

Artificial neural networks, mimicking human brains, exhibit great abilities in several tasks such as image recognition. Nowadays, most artificial neural networks rely on silicon-based general-purpose electronic circuits such as a central processing unit (CPU) and a graphics processing unit (GPU). However, in these circuits, a large amount of energy is consumed. Moreover, the absence of memory functionality in CPU and GPU is a disadvantage especially for recurrent-type artificial neural networks, in which past data is stored in the network as actual human brains. Therefore, developing devices specialized for brain-inspired computing, namely neuromorphic devices, are highly required. So far various neuromorphic computing models using spintronic devices have been proposed and demonstrated[1]. Among them, one of the promising models is a physical reservoir computing model. In the physical reservoir computing model, the input data are nonlinearly converted into multi-dimensional outputs by using nonlinear dynamics of spintronic devices. Incidentally, this nonlinear mapping of input data into the high-dimensional space is a key to neuromorphic computing; the mapping enables linearly inseparable data to be linearly separable, like the kernel method.

In this presentation, we demonstrate physical reservoir computing by using a magnetic-field induced nonlinear dynamics of skyrmions. A skyrmion is a particle-like topological spin structure and can be manipulated with low power consumption. Thus, skyrmions are expected to be applied to energy-saving devices. Moreover, skyrmions are theoretically predicted to show high performance in reservoir computing[2]. We use Pt/Co/Ir film deposited on $LiNbO_3$ substrate in which the formation of disordered skyrmion has been observed[3]. Our skyrmion-based physical device consists of parallelly connected Hall-bar shaped devices in which various constant magnetic field are applied (Fig. 1). In each Hall-bar device, we input a time-dependent out-of-plane magnetic field [$H_{AC}(t)$] whose waveform is the same as what we want to compute. The output is anomalous Hall voltage [$V^i(t)$] (Here, i denotes the output from i-th Hall bar); $V^i(t)$ changes in response to $H_{AC}(t)$ because of $H_{AC}(t)$-induced change in magnetic structures and is nonlinear with respect to $H_{AC}(t)$. In this way, the input signal is nonlinearly converted into multi-dimensional data set $\boldsymbol{V}(t) = [V^1(t), \cdots, V^N(t)]$. Then, the final output is calculated by a linear combination of $\boldsymbol{V}(t)$ (i.e. $\sum W_i V^i$), in which the coefficients (W_i) of the linear combination are optimized by using a training data set so that the final output is desirable.

We succeeded in a waveform recognition task, which is a conventional benchmark. Notably, the recognition rate of the skyrmion-based neuromorphic computing device is better than a neuromorphic computing device in which ferromagnetic-domain structures were used instead of skyrmions. This is attributed to a more complex nonlinear mapping and the larger number of the output dimension, both of which originate from the large degree of freedoms of the disordered skyrmion system such as the position and the size of skyrmions. Our results provide a guideline for developing energy-saving and high-performance neuromorphic computing devices with the use of skyrmions.

Reference

1) J. Grollier, et al., Nat. Electron. **3,** 360 (2020).
2) D. Prychynenko, et al., Phys. Rev. Appl. **9,** 014034 (2018).
3) T. Yokouchi, et al., Nat. Nanotech. **15,** 361 (2020).

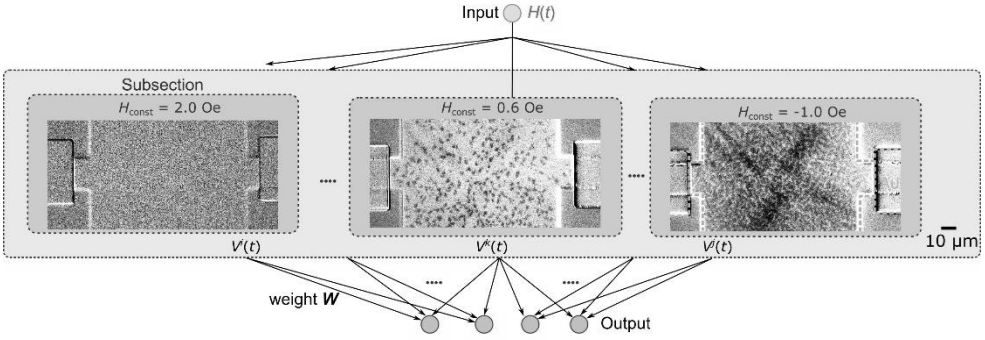

Fig. 1 Schematic illustration of a skyrmion-based neuromorphic computer. Polar Kerr images of Hall bar device with various constant magnetic field (H_{const}) are also presented.

Development of Domain Wall Type Spin Memristor toward Analogue Neuromorphic Computing

T. Shibata[1], T. Shinohara[1], T. Ashida[1], M. Ohta[1], K. Ito[1], S. Yamada[1], Y. Terasaki[1], and T. Sasaki[1]
[1]Advanced Products Development Center, TDK Corporation, Chiba 272-8558, Japan

Recent evolution of Artificial Intelligence (AI) is bringing drastic changes to society and industry. On the other hand, the rapid increase of its energy burden has become an urgent issue. From this viewpoint, an analogue neuromorphic computing have attracted much attention due to its extremely low-power and high-performance neural-network (NN) computing ability [1]. Memristors play key roles for realizing neuromorphic devices. It can store a synaptic weight of NN as an analog resistance state. For example, large-scale parallel multiply-accumulate (MAC) operation can be executed by applying an electric current flow to a memristor array. Memories-based spiking neural network devices have also been studied to accelerate the computational processing power with keeping power consumption. Phase change memory (PCM) and Resistive-RAM (ReRAM) are well-known elements in this field. A magnetic domain wall (DW) type memristor (spin-memristor) is another promising candidate for artificial synapses because of its typical conductance change behavior, non-volatility, high speed and high endurance operations. Numerical simulations show potential advantages of the spin-memristor [2]. However, an element-level development has not been well established. The elements have been well studied for a high-speed domain wall (DW) type MRAM, but not so much for memristors. In this presentation, we introduce our recent efforts to develop the spin-memristor for the neuromorphic application. The concept of the spin-memristor was verified by preparing a DW type magnetic tunneling junction (MTJ). Three-terminal top-pinned type MTJs were fabricated on a Si substrate. The stacking layer was Si wafer /buffer /DW layer /CoFeB Free layer /tunnel barrier /CoFeB Reference layer /synthetic antiferromagnetic (SAF) pinned layer. A pulse generator and a source measure unit are used for driving the DW and for measuring the resistance of MTJs. A linear and symmetric conductance response (Fig. 1), which was desirable for the artificial synapse, was experimentally demonstrated in the element level as expected [3]. A good NN computation adaptability was confirmed using a numerical simulation with its simplified element model. In addition, we also developed a 3-terminal element having SAF-type magnetic fixed layer at the one side of DW layer (Fig. 2), and successfully controlled the element initialization process just by applying an external magnetic field [4]. Since this structure allows us to initialize multiple elements by a simple procedure, it becomes helpful to realize an array level system and a mass-production in the future. The prototype element suggested a low power operation potential which may be at least comparable to other memristive elements such as PCM and ReRAM.

References

1) G. W. Burr *et al.*, Adv. Phys. X **2**, 89 (2017)
2) A. Sengupta *et al.*, IEEE Trans. Biomed. Circuits Syst. **10**, 1152 (2016)
3) T. Shibata *et al.*, Appl. Phys. Express **13**, 043004 (2020)
4) T. Ashida *et al.*, Jpn. J. Appl. Phys. **59**, 078002 (2020)

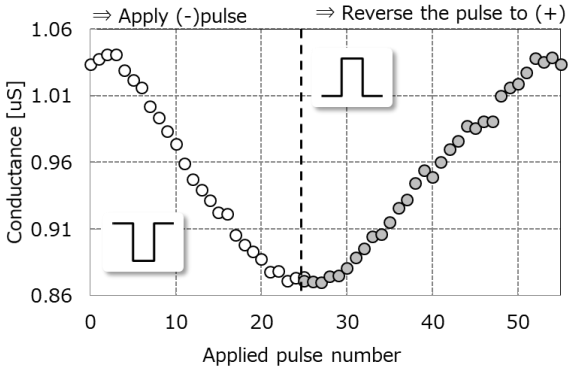

Fig.1 Symmetric conductance response as a function of driving current pulse

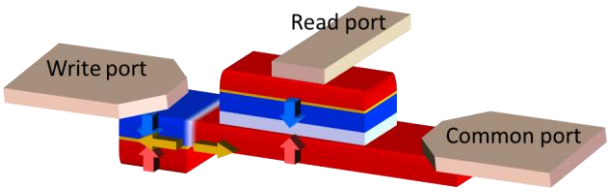

Fig.2 Schematic illustration of the element with SAF-type magnetic fixed layer

Strong magnon-magnon coupling in synthetic antiferromagnets

Yoichi Shiota[1], Tomohiro Taniguichi[2], Mio Ishibashi[1], Takahiro Moriyama[1], and Teruo Ono[1,3]
[1]Institute for Chemical Research, Kyoto University
[2]National Institute of Advanced Industrial Science and Technology (AIST), Spintronic Research Center
[3]Center for Spintronics Research Network, Graduate School of Engineering Science, Osaka University

Spin waves and their quasiparticles, i.e., magnons, can be used as information carriers and for information processing[1-3]. Hybrid quantum systems based on magnon have been intensively studied in the last decade, because these systems offer a promising platform for novel quantum information technologies[4]. It has been recently reported that an anticrossing gap between two magnetic resonances, so-called a magnon-magnon coupling, can be realized in several kinds of systems[5-8], which is analogous to the hybrid quantum system. However, most of experiments focused on magnons with uniform precession ($k = 0.0\ \mu\mathrm{m}^{-1}$, where k is the wave number). In this study we demonstrate the strong magnon-magnon coupling between acoustic and optic modes by utilizing magnons with nonuniform precession ($k \neq 0.0\ \mu\mathrm{m}^{-1}$) in ferromagnetic-metal-based synthetic antiferromagnets (SAFs) of FeCoB/Ru/FeCoB[9].

Figures 1(a)-1(c) shows the spin wave resonance spectra ($k = 1.2\ \mu\mathrm{m}^{-1}$) at $\varphi_k = 0°, 45°,$ and $90°$, where φ_k is the angle between an external magnetic field and the spin wave propagation direction. The anticrossing gap g/π between two modes appears when the spin wave propagates in the direction of $\varphi_k \neq 0°$ and is maximized at approximately $\varphi_k = 45°$. We found that the coupling strength is larger than the dissipation rates for both the resonance modes. Therefore, strong coupling regime is achieved in this study. A theoretical analysis shows quantitative agreements with the experimental results and indicates that the appearance of the anticrossing gap accompanies symmetry breaking with respect to the exchange of magnetizations due to dynamic dipolar interaction generated by the magnetization motion of spin waves. Our study offers a new approach toward tunable magnon-magnon coupling systems for SAF-based magnonic applications.

This work was supported by the JSPS KAKENHI Grans Nos. JP15H05702, 15K21752, JP16H05977, JP18K19021, 20K15161, JP20H00332, and ISHIZUE of Kyoto University Research Development Program.

Reference

1) V.V. Kruglyak *et al., J. Phys. D. Appl. Phys.* **43**, 264001 (2010)
2) A. Khitun *et al., J. Phys. D. Appl. Phys.* **43**, 264005 (2010)
3) A.V. Chumak *et al., Nat. Phys.* **11**, 453-461 (2015)
4) D. Lachance-Quirion *et al., Appl. Phys. Express* **12**, 070101 (2019)
5) S. Klingler *et al., Phys. Rev. Lett.* **120**, 127201 (2018)
6) J. Chen *et al., Phys. Rev. Lett.* **120**, 217202 (2018)
7) D. MacNeill *et al., Phys. Rev. Lett.* **123**, 047204 (2019)
8) L. Liensberger *et al., Phys. Rev. Lett.* **123**, 117204 (2019)
9) Y. Shiota *et al., Phys. Rev. Lett.* **125**, 017203 (2020)

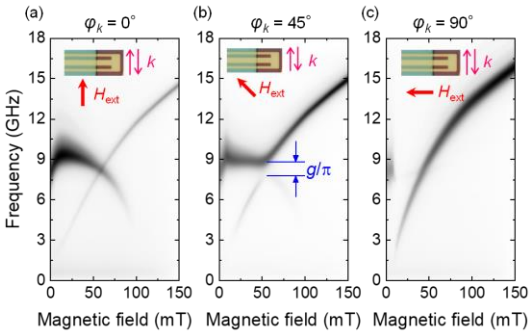

Fig. 1 Contour plots of Re[S_{11}] for spin wave resonance spectra ($k = 1.2\ \mu\mathrm{m}^{-1}$) at (a) $\varphi_k = 0°$, (b) $45°$, and (c) $90°$.

Measurement and control of spin quantum states utilizing semiconductor quantum dots

T. Otsuka[1,2,3], T. Nakajima[3], M. R. Delbecq[3], P. Stano[3,4], S. Amaha[3], J. Yoneda[3], K. Takeda[3], G. Allison[3], S. Li[3], A. Noiri[3], T. Ito[3], D. Loss[3,5], A. Ludwig[6], A. D. Wieck[6], and S. Tarucha[3]
[1]Research Institute of Electrical Communication, Tohoku University, Sendai 980-8577, Japan
[2]Center for Science and Innovation in Spintronics, Tohoku University, Sendai 980-8577, Japan
[3]Center for Emergent Matter Science, RIKEN, 2-1 Hirosawa, Wako, Saitama 351-0198, Japan
[4]Institute of Physics, Slovak Academy of Sciences, 845 11 Bratislava, Slovakia
[5]Department of Physics, University of Basel, Klingelbergstrasse 82, 4056 Basel
[6]Lehrstuhl für Angewandte Festkörperphysik, Ruhr-Universität Bochum, D-44780 Bochum, Germany

Spin phenomena in semiconductor nanostructures are attractive targets in basic science and important in device applications. Semiconductor quantum dots (QDs) are nanostructures which confine electrons in small regions and work as artificial and controllable quantum states. They can handle single-electron spins. Single-electron spins in QDs are simple spin systems, show quantum mechanical properties, and nowadays are considered as a good candidate for quantum bits in quantum information processing. By utilizing the semiconductor QDs, we can measure and control the single-electron spin states.

To measure the single-electron spins in semiconductor nanostructures, local spin probes which can directly access the spin states are useful. We can realize such probes using semiconductor QDs. We can get the information of the spin states by analyzing the electron tunneling into spin-selective levels formed in the QDs which couple to the target structures. We can also measure the dynamics of the local electronic states by high-speed electric measurements utilizing high-frequency techniques called RF reflectometry. We measure the dynamics of the local single-electron spin and charge states in a semiconductor nanostructure which consists of a QD and an open electronic reservoir. This hybrid system is a simple model of an open quantum system. The change of the local spin and charge states inside of the target QD induced by the interaction between the QD and the reservoir is detected by the local probe. The relaxation times are different between the spin and the charge states. The observed difference is reproduced by a theoretical model treating the tunneling process [1].

Control of single-electron spin states is an essential operation of semiconductor quantum bits utilizing single-electron spins in QDs. The spins have relatively long quantum coherence times in solid-state devices. The control is realized by electron-spin resonances induced by the oscillatory shifts of the QD position by microwave's electric fields and the magnetic field gradient created by micro-magnets. We realize and improve the operation of the single-electron spins by optimizing the device structures and materials. We also fabricate the semiconductor multiple QD devices towards larger quantum bit systems. Scale-up of the quantum bit systems is important to realize larger-scale quantum algorithms. We demonstrate charge state control and single-spin operations in the scaled-up devices [2]. These results are important in the understanding of spin phenomena in semiconductor nanostructures and device applications like semiconductor quantum sensors and qubits.

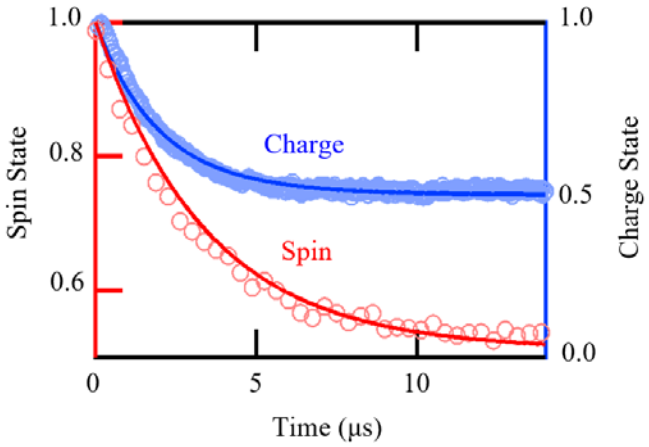

Fig. 1. Measured dynamics of the spin and charge states by a semiconductor quantum dot sensor.

Reference

1) T. Otsuka, T. Nakajima, M. R. Delbecq, P. Stano, S. Amaha, J. Yoneda, K. Takeda, G. Allison, S. Li, A. Noiri, T. Ito, D. Loss, A. Ludwig, A. D. Wieck, and S. Tarucha, Phys. Rev. B 99, 085402 (2019).
2) T. Ito, T. Otsuka, T. Nakajima, M. R. Delbecq, S. Amaha, J. Yoneda, K. Takeda, A. Noiri, G. Allison, A. Ludwig, A. D. Wieck, and S. Tarucha, Appl. Phys. Lett. 113, 093102 (2018).

Majorana fermions and non-Abelian anyons in a Kitaev quantum spin liquid

Yuichi Kasahara
Department of Physics, Kyoto University, Kyoto 606-8502, Japan

Quantum spin liquid (QSL) is a novel state of matter that lacks long-range magnetic order all the way down to zero temperature while possesses some special patterns of quantum mechanical entanglement. The long-standing experimental challenges associated with the identification of the QSL state is the detection of fractionalized excitations, which are signatures of topological order inherent to the QSL. Recently, the Kitaev spin model of insulating magnets on two-dimensional (2D) honeycomb lattice has attracted interest, as it hosts a QSL where quantum spins are fractionalized into Majorana fermions.[1] In magnetic fields, the emergence of Majorana edge current and non-Abelian anyons in the bulk is predicted to manifest itself in the form of thermal quantum Hall effect, a feature discussed in topological superconductors and even-denominator fractional quantum Hall state. Here we report on thermal Hall conductivity κ_{xy} measurements in α-$RuCl_3$, a candidate material for Kitaev QSL on a 2D honeycomb lattice.[2,3] In magnetic field perpendicular to the 2D honeycomb planes, positive κ_{xy} develops in a spin-liquid state below the temperature characterized by the Kitaev interaction $J_K/k_B \sim 80$ K, demonstrating the presence of highly unusual itinerant excitations. Although the zero-temperature property is masked by the antiferromagnetic (AFM) ordering at $T_N = 7$ K, the sign, magnitude, and T-dependence of κ_{xy} at $T_N < T < J_K/k_B$ follows the predicted trend of the itinerant Majorana fermion excitations.[2] The application of a tilted magnetic field suppresses the AFM order, leading to a field-induced QSL ground state. In this QSL state, the 2D thermal Hall conductance per honeycomb plane κ_{xy}^{2D}/T shows a plateau behavior as a function of applied magnetic field and has a quantization value of $(\pi^2/6)(k_B^2/h)$, which is exactly half of κ_{xy}^{2D}/T in the integer quantum Hall state and conventional odd-denominator fractional quantum Hall state that hosts Abelian anyons.[4] We also show that the half-integer thermal Hall plateau is observed even when the magnetic field is applied parallel to the 2D plane. In addition, the topological Chern number determined by the sign of the quantized thermal Hall conductance is consistent with that expected in the Kitaev QSL.[5] These results provide strong evidence of topologically protected chiral currents of charge neutral Majorana fermions at the edge and and non-Abelian anyons in the bulk of the crystal.[3] Above a critical field, the quantization disappears and κ_{xy}^{2D}/T goes to zero rapidly, indicating a topological phase transition.

This work is in collaboration with T. Ohnishi, Sixiao Ma, Y. Matsuda (Kyoto Univ.), K. Sugii, M. Shimozawa, M. Yamashita, Y. Mizukami, O. Tanaka, Y. Motome, T. Shibauchi (Univ. of Tokyo), N. Kurita, H. Tanaka (Tokyo Institute of Technology), and J. Nasu (Yokohama National University).

References

1) A. Kitaev, Ann. Phys. **321**, 2 (2006).
2) Y. Kasahara, K. Sugii *et al*., Phys. Rev. Lett. **120**, 217205 (2018).
3) Y. Kasahara *et al*., Nature **559**, 227 (2018).
4) M. Banerjee *et al*., Nature **545**, 75 (2017).
5) T. Yokoi *et al*., arXiv:2001.01899 (2020).

強磁性共鳴による Co-Fe 合金単層膜自己誘起逆スピンホール効果

白　承根、手木　芳男*、仕幸　英治
(阪市大院工、*阪市大院理)

Self-induced inverse spin-Hall effect in Co-Fe alloy single-layer films under the ferromagnetic resonance

S.K. Baek, Y. Teki*, E. Shikoh
(Osaka City Univ. Eng., *Osaka City Univ. Sci.)

はじめに

近年、強磁性共鳴(FMR)の下で強磁性体の単層薄膜に生じる自己誘起逆スピンホール効果による起電力の生成が注目されている[1-3]。Fig. 1 に強磁性薄膜内の局在磁気モーメントの、FMR 下における動的特性の概要を示す。強磁性膜の上面側(空気層側)と下面側(基板側)との間で局在磁気モーメントの減衰特性が異なるため、膜の面直方向に純スピン流が生成され、その純スピン流は逆スピンホール効果(ISHE)[4]によって起電力に変換されると考えられている[2]。これまでに Fe, Co, および $Ni_{80}Fe_{20}$ の自己誘起 ISHE による起電力の生成が達成された[1-3]。しかしながら元素により起電力特性が異なった。本研究では FMR 下の Co-Fe 合金の単層膜における自己誘起 ISHE による起電力の生成を達成し、その Co と Fe の組成比依存性を評価した。

実験方法

電子ビーム蒸着法により、熱酸化膜付き Si 基板上に Co_xFe_{100-x} 合金(x = 0, 25, 50, 75, 100)の単層膜(膜厚 25 nm)を作製した。FMR の励起には ESR 装置を用いる方法と、電磁石による静磁界、およびネットワークアナライザによる高周波電流を伝送線路に印加することによって生成される高周波磁界を用いる方法を併用した。起電力の検出にはナノボルトメータを用いた。全ての測定は室温で行った。

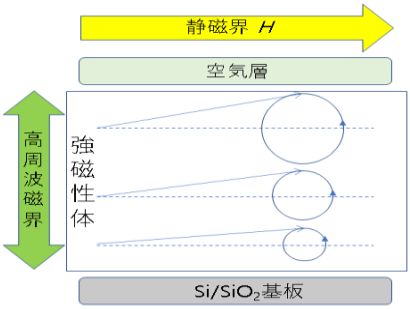

Fig. 1. Spin current generation mechanism in a ferromagnetic metal film under the FMR.

実験結果

Fig. 2 に x = 75 の試料における FMR 下の起電力特性を示す。高周波の出力は 200 mW である。共鳴磁界付近において起電力が観測され、起電力の符号は静磁界の方向を逆転するとことにより、反転した。従来の解析手法[4]により、起電力の起源は主に ISHE であると結論付けた。Fig. 3 に伝送線路を用いて評価した、Co-Fe 合金薄膜における FMR 下の ISHE による起電力の Co 濃度依存性を示す。高周波の出力は 20 mW である。組成の異なる各試料において静磁場に対する反転対称性を示す出力電圧特性が観測された。更に起電力は高周波出力に依存した。以上により ISHE[4]によって起電力が発生したと結論付けた。即ち Co-Fe 合金薄膜においても FMR 下で ISHE による起電力の生成を達成した。学会時には以上の詳細を議論する。

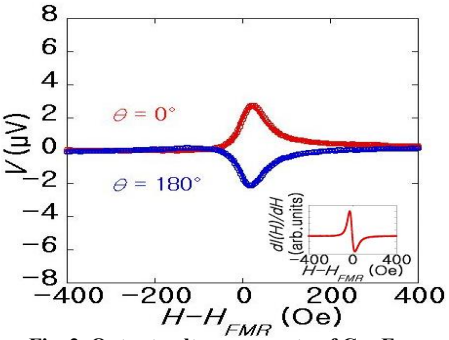

Fig. 2. Output voltage property of $Co_{75}Fe_{25}$ under FMR. (Inset) an FMR spectrum.

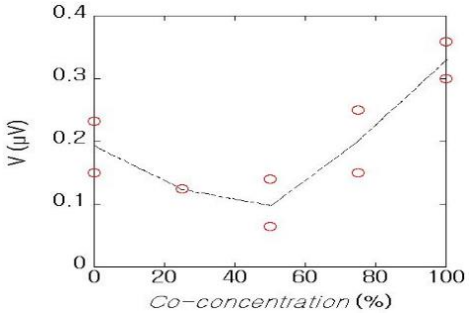

Fig. 3. Co concentration dependence of the output voltage due to the ISHE.

参考文献

[1] A. Tsukahara, et al., Phys. Rev. B **89**, 235317 (2014).
[2] K. Kanagawa, et al., AIP Adv. **8**, 055910 (2018).
[3] O. Gladii, et al., Phys. Rev. B **100**, 174409 (2019).
[4] E. Saitoh, et al., Appl. Phys. Lett. **88**, 182509 (2006).

スロット線路を用いたイットリウム鉄ガーネットの磁化ダイナミクス励起とスピン波の検出

神田哲典、室賀翔[1]、遠藤恭[2]
（大島商船高専、[1]秋田大、[2]東北大）

Magnetization dynamics induced by slot line waveguide and detection of spin waves in yttrium iron garnet

T. Koda, S. Muroga[1], Y. Endo[2]
(National Inst. of Technology, Oshima College, [1]Akita Univ., [2]Tohoku Univ.)

はじめに

我々はイットリウム鉄ガーネット(YIG)の磁化ダイナミクスを励起する高周波伝送線路としてスロット線路に着目し、高周波応答の線路形状依存性を評価した。その結果、スロット線路の間隔に依存する磁化ダイナミクスが励起されることを見出した[1]。マイクロマグネティクスシミュレーションによる解析から線路から発生するスピン波と磁化ダイナミクスの相互作用が存在することが示唆された。そこで、その高周波応答とスロット線路から発生するスピン波の相関を検討したので報告する。

実験方法

試料には(111)ガドリウムガリウムガーネット（GGG）単結晶基板上に液相エピタキシャル法で成長された膜厚 10 μm の YIG(111)単結晶膜を用いた。試料上に高周波伝送線路として、フォトリソグラフィー法で非対称型のコプレーナウェーブ伝送線路、および、スロット伝送線路を形成した。0 dBm の高周波電力をこの伝送線路により YIG 上に入力し、反射電力強度の外部磁界依存性をネットワークアナライザで評価した。また、試料上にスピン波を検出するための非対称型コプレーナウェーブ線路を 1 mm 離した位置に設置し、YIG を伝搬するスピン波をアンテナ法により検出・評価した。

実験結果

図 1 には信号線路幅 10 μm、線路幅間隔 55 μm のスロット線路における測定結果を示す。入力周波数は 7.2 GHz である。反射強度は 1670 Oe および 1730 Oe 付近に吸収ピークが確認される。マイクロマグネティクスによる解析から、スロット線路のそれぞれの線路周辺で局所的に磁化歳差運動が誘起され、スピン波が伝搬することが示唆されている。実際、アンテナ法においてもスピン波に起因する信号が検出されている。1730 Oe 付近の吸収ピークよりも高磁場側においては、アンテナ法で検出されたスピン波の強度と吸収ピーク強度に大きな相関は見られなかった。一方、1700 Oe 近傍の挙動で、高周波電力の吸収強度が少ない磁場領域ではスピン波の検出出力が極小値を示しており、磁化歳差運動とスピン波強度に強い相関を示した。本試料で発生するスピン波は表面静磁波であり、その波長は同一周波数の場合、磁場の低下と共に短くなる。1700 Oe におけるスピン波の波長はおよそ 55 μm と見積もられる。電磁界解析より、伝送線路間の高周波磁場の位相は 180° ずれているため、このスピン波の波長において、スピン波と局所磁化歳差運動が逆位相の関係になり磁化歳差運動のスピン波が抑制されたと考えられる。すなわち、この結果はスピン波が局所磁化歳差運動に影響を及ぼしていることを強く示唆する結果と考えられる。講演では磁化歳差運動とスピン波の相関の素子サイズ依存性を中心に報告する。

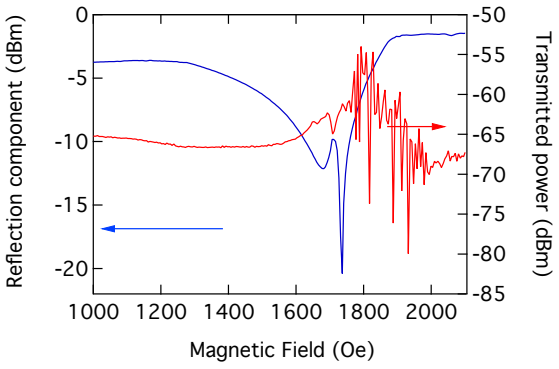

Fig.1. Magnetic field dependence of reflection component of input power and transmitted power for the detection of spin waves.

謝辞　本研究にあたり、株式会社グラノプトから測定試料の御協力を頂きました。本研究の一部は，JSPS 科研費 No.18K14114 の助成を受けて行われた

参考文献　[1] Koda et.al., Appl. Phys. Lett., vol. 116 102403 (2020).

準周期マグノニック結晶を用いたMSSWの非相反性制御

藤井幹太, 笠原健司, 眞砂卓史
（福岡大理）

Propagation properties of spin waves in magnonic crystal with quasi periodic structure

K. Fujii, K. Kasahara, and T. Manago
(Fukuoka Univ.)

はじめに　近年、強磁性体導波路中に周期的な構造を導入したマグノニック結晶(MC)を用いて、スピン波の伝搬特性を制御しようとする研究が精力的に行われている。これまでに我々は、強磁性体金属のパーマロイ(Py)に周期的な溝を導入したMCを作製し、アンテナを用いた電気的手法により特定の周波数帯でスピン波が伝搬できないマグノニックバンドギャップの観測に成功した[1]。長期的な周期性を持たない準周期構造のMCは通常のMCにはない伝搬特性を示すことが期待されるものの、その調査はほとんど行われていない。本研究ではマイクロマグネティックシミュレーションを用い、準周期構造をもつ1次元のPy MC中を伝搬する静磁表面波(MSSW)の伝搬特性を調査した。

計算方法　スピン波の伝搬特性の計算は、Object Oriented Micromagnetic Framework(OOMMF)により行った。縦×横×膜厚が102.4 μm × 6 μm × 75 nmであるPy導波路を仮定し、深さが25 nmで溝の幅 d が0.8 μmの溝と凸の幅が$\frac{1+\sqrt{5}}{2}$ dの凸を、漸化式 $A_{n+2} = A_{n+1} + A_n$ で表されるフィボナッチ数列に従い、Pyの長辺方向に導入した(Fig.1)。+y方向の印加静磁場に対して、右側に伝搬する方向をForward、それと逆方向をReverseと定義した。スピン波励起用のシグナル(S)とグラウンド(G)アンテナの磁場分布はMATLABで行った。S及びGアンテナ幅は、それぞれ1.0及び50 μmで、SG間距離は1.0 μm、それらの厚みは205 nmとした。この磁場分布をOOMMFに取り込み、パルス幅が50 psのガウシアンパルスを印可することにより、スピン波を励起した。静磁場の印可方向はPyの短辺方向(20 mT)としているため、伝搬するスピン波はMSSWモードとなる。

実験結果　Figure 2は、励起アンテナからの距離が 40 μmのときのスピン波のスペクトルである。赤と青はそれぞれ、+y方向の印加静磁場に対して、右側に伝搬する方向(Forward)と、それと逆向き(Reverse)のスペクトルを示している。構造のないPy膜において+y方向に磁化が向いている場合、アンテナ法で励起されたMSSWは、－x方向に比べ、+x方向の強度が大きくなる非相反性を示すことがよく知られている。4 ～ 8 GHz付近では、赤(+x方向)のスペクトル強度が青(－x方向)の強度より大きく、典型的なMSSWモードの非相反性が現れているが、8 ～ 10 GHz付近では、赤と青のスペクトル強度が逆転しており、非相反性が逆転する現象が観測された。これは準周期構造によりMSSWモードの非相反性が変化したことを示している。

参考文献　[1] Koji Shibata, Kenji Kasahara, and Takashi Manago. Applied Physics Express **12**, 053002 (2019).

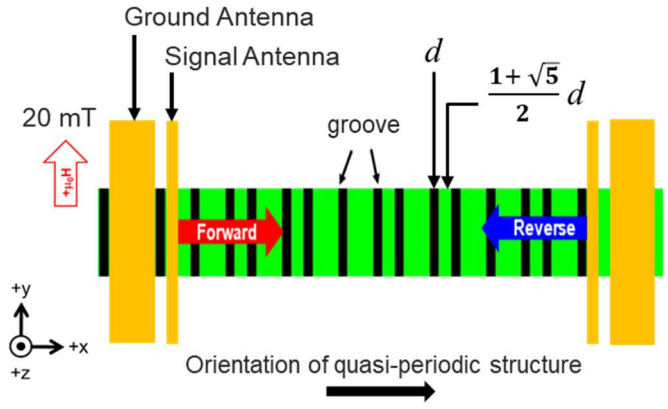

Fig.1 Schematic illustration of a quasi-periodic Py MC.

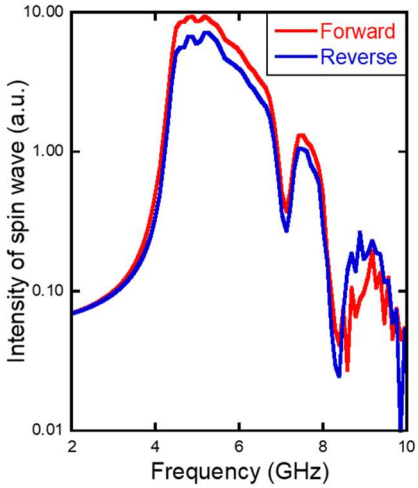

Fig.2 Spin wave spectra for forward and reverse direction of a quasi-periodic Py MC.

Spin Wave Resonance in Perpendicularly Magnetized Synthetic Antiferromagnets

Mio Ishibashi[1], Yoichi Shiota[1], Shinsaku Funada[1], Takahiro Moriyama[1], and Teruo Ono[1,2]

[1]*Institute for Chemical Research, Kyoto University, Gokasho, Uji, Kyoto 611-0011, Japan*

[2]*Center for Spintronics Research Network, Graduate School of Engineering Science, Osaka University, Toyonaka, Osaka 560-8531, Japan*

Spin wave polarization, i.e. the rotation direction of magnetic moments around an applied magnetic field, has been attracted much attention for a new freedom degree of spin waves in addition to spin wave amplitude and phase. Unlike ferromagnetic spin waves, antiferromagnetic spin waves in colinear antiferromagnets have both right and left-handed polarizations [1,2]. However, spin waves in crystal antiferromagnets have high resonance frequency of THz regime due to strong exchange coupling, which can cause difficulties in excitation or manipulation of spin waves. In this study, we experimentally demonstrate spin wave resonance in perpendicularly magnetized synthetic antiferromagnets by spectroscopy using a vector network analyzer.

Films of Ta(3.0)/Pt(2.0)/[Co(0.2)/Ni(0.7)]$_5$/Co(0.2)/Ru(0.5)/Co(0.2)/[Co(0.2)/Ni(0.7)]$_5$/Ru(3.0) (thickness in nm) were deposited using dc magnetron sputtering on thermally oxidized Si substrates. The films were fabricated to devices for spin-wave-spectroscopy as shown in Fig. 1 (a). Figure 1 (b) shows a contour plot of spin wave resonance spectra (k = 1.2 μm) generated from Re[S_{11}] spectra measured at a given out-of-plane bias magnetic field. The applied magnetic field swept from +250 mT to –250 mT with a step of 10 mT. Two resonance modes were observed from 130 mT to - 190 mT, where the two magnetic moments were antiferromagnetically aligned. These two resonance frequencies increase and decrease linearly with the bias magnetic field, which indicates excitation of right and left-handed polarized spin waves. In the presentation, we will discuss more details with theoretical analysis based on the equation of motion.

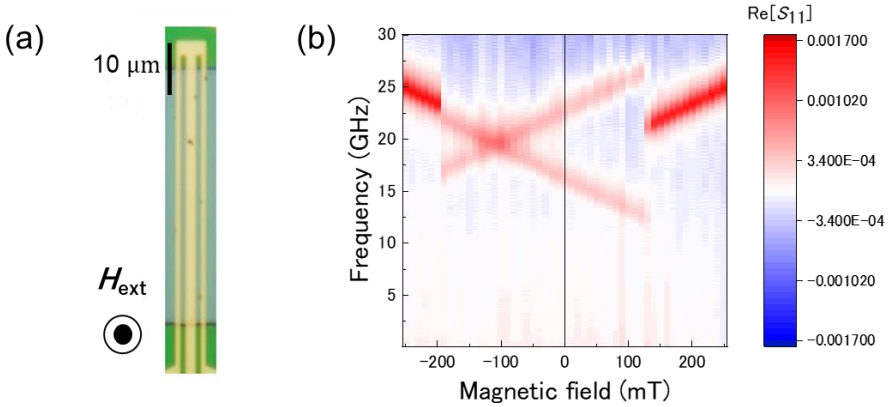

Fig.1 (a) Optical micrograph of the device. (b) Contour plot of Re[S_{11}] spectra.

[1] F. Keffer and C. Kittel, Phys. Rev. **85**, 329 (1952).

[2] F. Keffer, H. Kaplan, and Y. Yafet, Am. J. Phys. **21**, 250 (1953).

Co/Pt 多層膜のコプラナー導波路強磁性共鳴

冨田知志、菊池伸明、畑山正寿、岡本聡
（東北大）

Co-planar waveguide ferromagnetic resonance of Co/Pt multilayers

Satoshi Tomita, Nobuaki Kikuchi, Masatoshi Hatayama, Satoshi Okamoto
(Tohoku Univ.)

はじめに

Co/Pt 多層膜は垂直磁気異方性を持つことから、これまで記録媒体やメモリの観点から精力的に研究されてきた [1]。一方で人工磁性体という点からは、Co 膜厚と Pt 膜厚というふたつの自由度を持つため、これらを変化させることで多層膜の磁気特性が制御できることが興味深い。例えば多層膜の g 値が制御できた暁には人工フェリ磁性構造での角運動量補償が可能となり [2]、スピン波デバイスなど新たな応用への可能性が広がると期待される [3]。しかしながらこれらの自由度が具体的に多層膜の g 値やダンピングにどのような影響を与えるかは明らかではない。そこで今回我々は Co 膜厚を変化させた Co/Pt 多層膜を作製し、コプラナー導波路（CPW）を用いた強磁性共鳴（FMR）を測定し、g 値やダンピングを調べる。

実験方法

多層膜はマルチターゲット DC スパッタリング法で作製する。基板は石英基板を用いる。まず下地層として Ta を 1nm、更に Pt を 2nm 成膜する。その上に Co（膜厚 Xnm）と Pt（膜厚 0.3nm）を 10 周期積層して Co/Pt 多層膜とし、最後に 1.7nm の Pt でキャップする。Co 膜厚の X が 0.3、0.6、0.9、1.2、1.5 の 5 種類の試料を作製した。

CPW を作製する前に、多層膜をフォトリソグラフィと Ar イオンエッチングで幅 10μm、長さ 1.5mm の短冊状に加工し、厚さ 100nm の SiO_2 スペーサーを堆積する。Co/Pt 多層膜の短冊の上に CPW の信号線が載るようフォトリソグラフィを行い、Cr を 5nm、Au を 200nm、Cr を 5nm スパッタ成膜し、リフトオフを経て CPW を作製する。CPW の信号線の幅は 10μm である。

CPW を高周波プローブと同軸ケーブルを介してベクトルネットワークアナライザに接続する。マイクロ波の透過率に対応する S パラメータの S_{21} を測定し、絶対値$|S_{21}|^2$ を得る。外部直流磁場は面直方向に印加する。特定の磁場で測定する直前に 1.5T でバックグラウンドスペクトルを測定して差し引く。すると差分の$|S_{21}|^2$ スペクトルに FMR 信号が吸収（ディップ）として現れる。

結果と考察

図に X=0.9 の試料の CPW-FMR スペクトルを示す。面直方向の外部直流磁場を 0.1T から 1.0T まで変化させている。図のスペクトルに現れるディップは、磁場の大きさを増加させると高周波にシフトすることから、FMR 信号であると考えられる。これらスペクトルのディップをローレンツ関数でピーク分離し、外部磁場に対する共鳴周波数のプロットから g 値が、共鳴周波数に対する半値幅のプロットからダンピング定数が得られる。講演では g 値やダンピング定数の、Co 膜厚（X）依存性について解析した結果を報告する。本研究は科研費（20H01911）により支援された。

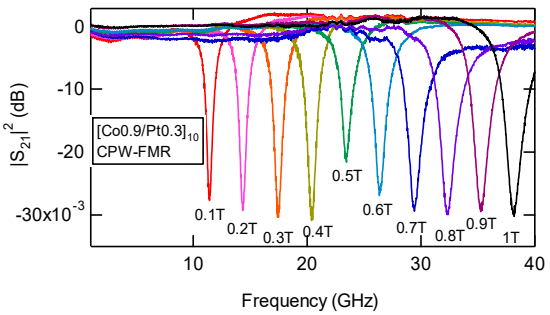

Fig. CPW-FMR spectra of a $[Co0.9/Pt0.3]_{10}$ multilayer sample at various magnetic fields.

参考文献

1) Yakushiji et al., APEX 8, 083003 (2015).
2) Fukuda et al., APEX 13, 063003 (2020).
3) Roldan-Molina et al., PRL 118, 061301 (2017).

磁性ナノ粒子の構造に依存した磁気緩和の評価

大多哲史[1], 宮澤良真[1], 永田大貴[2], 二川雅登[1], 竹村泰司[2]
([1]静岡大学, [2]横浜国立大学)

Evaluation of magnetic relaxations of magnetic nanoparticles depended on particle structure

S. Ota[1], R. Mayazawa[1], D. Nagata[2], M. Futagawa[1], and Y. Takemura[2]
([1]Shizuoka University, [2]Yokohama National University)

はじめに

磁性ナノ粒子のがん温熱治療や磁気粒子イメージング(Magnetic particle imaging: MPI)といった医療応用を考える際に、磁気緩和の評価は必要不可欠である。著者らは、シングルコア、マルチコア、鎖状構造の磁性ナノ粒子について、交流磁化計測を実施し、双極子相互作用の影響で磁気異方性がマルチコア構造では低下、鎖状構造では実行的に増加することを示した[1)]。また、高速で応答するパルス磁場を印加することで、磁化の緩和過程を実験的に観測し、ネール緩和の後にブラウン緩和が生じる二段階の緩和現象を観測した[2)]。本研究では、超常磁性的なシングルコア（S1)、マルチコア（S2)、ナノフラワー（S3)、強磁性的なシングルコア（S4)、立方構造（S5）という異なる 5 つの構造の粒子について、磁気緩和特性を評価した。

実験方法・結果

粒子の物理的回転を生じないよう樹脂で固定した固体試料と、純水中に分散した液体試料を各粒子に関して用意した。超常磁性的なシングルコア構造（CMEADM-004)、マルチコア構造（Ferucarbotran）構造の粒子は名糖産業株式会社から提供いただいた。ナノフラワー構造（synomag®-D)、立方構造（BNF-starch）の粒子は Micromod 社から、強磁性的なシングルコア構造（M-300）はシグマハイケミカル社から購入した。講演で載せる磁性ナノ粒子の透過型電子顕微鏡像は、横浜国立大学機器分析センターに測定いただいた。

Fig. 1 に振動試料型磁力計（VSM）で測定した直流磁化曲線を示した。直流磁化曲線に関して、固体試料では、S1, S2, S3 では保磁力が確認されないが、S4, S5 について保磁力が確認された。これは S4, S5 が強磁性的であることを示している。液体試料では、粒子回転が生じるため、構造に関係なく超常磁性的であった。さらに超常磁性的な構造の中でも S2, S3 に対して S1 は、固体試料と液体試料の磁化曲線が酷似していた。これはマルチコア構造やナノフラワー構造において、集合することで磁気異方性が低下する一方で、実効的にコア粒径が増加している影響[1,3,4)]で、異方性エネルギーが増加するためである。講演では、交流磁化曲線から解析した磁気緩和に関する計測結果について詳細に述べる。

謝辞

本研究の一部は、科研費 20H00238、20H02163 の助成を受けて実施した。

参考文献

1) S. Ota, Y. Matsugi, T. Nakamura, R. Takeda, Y. Takemura, I. Kato, S. Nohara, T. Sasayama, T. Yoshida, K. Enpuku, *J. Magn. Magn. Mater.*, 474, 311–318 (2019).
2) S. Ota, and Y. Takemura, *J. Phys. Chem. C*, **123**, 28859−28866 (2019).
3) T. Yoshida, N. B. Othman, K. Enpuku, *J. Appl. Phys.*, **114**, 173908 (2013).
4) P. Bender, J. Fock, C. Frandsen, M. F. Hansen, C. Balceris, F. Ludwig, O. Posth, E. Wetterskog, L. K. Bogart, P. Southern, W. Szczerba, L. Zeng, K. Witte, C. Grüttner, F. Westphal, D. Honecker, D. González-Alonso, L. F. Barquín, C. Johansson, *J. Phys. Chem. C*, **122**, 3068−3077 (2018).

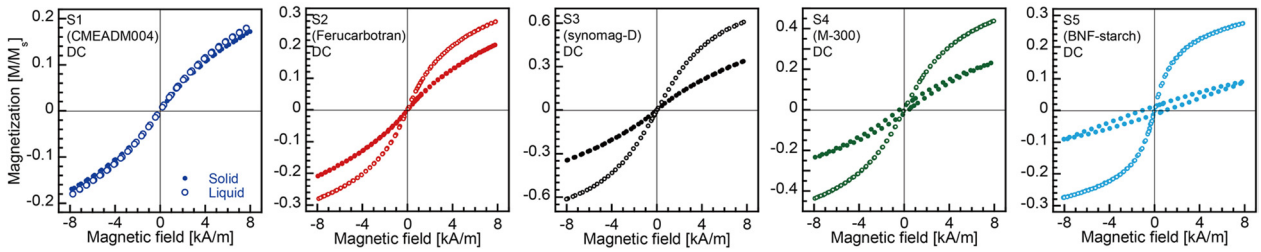

Fig. 1　Magnetization curves of measured magnetic nanoparticles in solid and liquid under DC magnetic field.

Cuマトリクス中に配向する単結晶強磁性ナノキューブの結晶磁気異方性の評価

小林昌太[1]、山南豪[1]、坂倉響[1]、竹田真帆人[1]、山田努[1]、佐久間洋志[2]、
Suko Bagus Trisnanto[1]、大多哲史[3]、竹村泰司[1]
([1]横浜国立大学、[2]宇都宮大学、[3]静岡大学)

Evaluation of magnetocrystalline anisotropy of oriented ferromagnetic single crystal nanocube in copper matrix

Shota Kobayashi[1], Tsuyoshi Yamaminami[1], Hibiki Sakakura[1], Mahoto Takeda[1], Tsutomu Yamada[1], Hiroshi Sakuma[2], Suko Bagus Trisnanto[1], Satoshi Ota[3], Yasushi Takemura[1]
([1]Yokohama National University, [2]Utsunomiya University, [3]Shizuoka University)

はじめに

磁性ナノ粒子を用いた磁気ハイパーサーミア治療において、交流磁場中における磁性ナノ粒子の発熱効率の向上のため、磁化特性の解明が重要である。本研究では、単結晶磁性ナノキューブ NiFe-Cu についての磁化測定を行うことにより、結晶磁気異方性に由来する磁化特性を観測することに成功した。

実験方法

本研究では Fig. 1 に示すように、時効処理を施した単結晶合金 $Cu_{75}Ni_{20}Fe_5$ 中の<100>方向に配列して析出したナノキューブ NiFe-Cu [1,2]について、直流磁化測定を磁場強度 4-1200 kA/m、交流磁化測定を励磁周波数 1-100 kHz, 磁場強度 4 kA/m の条件で磁化特性の観測を行った。交流磁化測定においては、測定試料 $Cu_{75}Ni_{20}Fe_5$ に直流バイアス磁場 1200 kA/m を印加し NiFe-Cu の磁化を飽和させた状態で行い、渦電流による信号のみを検出し、直流磁場を印加しない場合との差分より NiFe-Cu の磁化のみを導出した。このとき、直流磁場は交流磁場と垂直に印加した。測定は試料の結晶方位<100>、<110>、<111>方向についてそれぞれ行った。

実験結果

直流磁化測定より得られた磁化曲線を Fig. 2 に示す。Figure 1 に示した TEM 図において、ナノキューブ NiFe-Cu が<100>方向に配列して析出していることから、<100>方向が磁化容易軸であるように見える。しかし、Fig. 2 に示すように<100>方向に磁場を印加したときに得られる磁化よりも、<111>方向に磁場を印加したときの方が磁化が大きいという結果が得られ、これは結晶磁気異方性に起因する磁化特性である。結晶磁気異方性による磁化特性評価の詳細[3]、及び交流磁化測定時の渦電流についての考察は当日発表する。

参考文献

1). Kim, *et al.*, *Jpn. J. Appl. Phys.*, **55**, 123002, 2016.
2). Matai, *et al.*, *Mater. Sci. Forum*, **941**, 1324, 2018.
3). Kobayashi, *et al.*, *molecules* **25**, 3282, 2020.

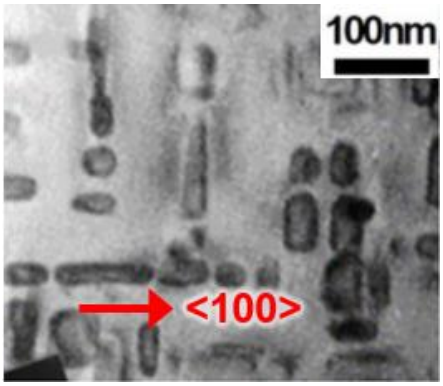

Fig. 1 Bright-field transmission electron micrograph and selected area electron diffraction pattern of the $Cu_{75}Ni_{20}Fe_5$ sample.

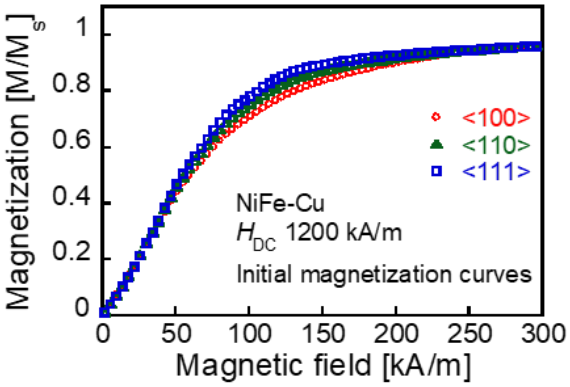

Fig. 2 Initial magnetization curves of the NiFe-Cu nanocubes recorded with the maximal DC magnetic field of 1200 kA/m.

三次元磁気粒子イメージングにおける液相・固相サンプル識別法の開発

野口裕希、吉田敬
（九州大学）

Development of Discrimination Method of Mobile and Immobilized Magnetic nanoparticle samples in 3D Magnetic Particle Imaging.

Yuki Noguchi, Takashi Yoshida
(Kyushu University)

1 はじめに

近年、磁気応用による医療診断技術が注目されており、その中の一つに粒子からの高調波信号を検出し対象の位置を特定する、磁気粒子イメージング(MPI)がある。本研究では、検査対象と結合した磁性ナノ粒子を「固相サンプル」、未結合の粒子を「液相サンプル」として疑似的に再現し、それぞれの高調波磁化特性の違いにより両者を三次元的に識別することを目指した。

2 原理

2.1 高調波磁化特性

液相サンプルと固相サンプルでは磁気緩和に違いが生じるため、励起されたサンプルに直流傾斜磁界をかけた際の高調波信号の減衰に差異が生じる。MPI では x, y, z 軸方向に直流傾斜磁界をかけているため、サンプル状態によって三次元的な信号の広がりに違いがでることになる。

本研究では、固相サンプルの磁化容易軸を交流励起磁界と同じ方向に揃えることでさらなる違いを生み、この違いを利用して識別を目指す。なお磁性ナノ粒子サンプルとして MS1 を用いた。

2.2 画像再構成

液相・固相サンプルからの第三高調波が混在した検出信号 v から、それぞれの空間分布 c_{liq} と c_{sol} を再構成する手法として、液相・固相サンプルのシステム行列以下に示す NNLS(Nonnegative Least Squares)法を用いる。

$$\text{minimize} \quad \left\| [A_{liq} \quad A_{sol}] \begin{bmatrix} c_{liq} \\ c_{sol} \end{bmatrix} - v \right\|^2 + \lambda \left\| \begin{bmatrix} c_{liq} \\ c_{sol} \end{bmatrix} \right\|^2$$

ここで、A_{liq},A_{sol} は、液相・固相サンプルのシステム行列である。

3 実験結果

サンプル容器のサイズは、直径 6 mm、深さ 13 mm の物を使用した。液相サンプルは MS1 を 10.8 μL に精製水 139.2 μL を加えて作成し、固相サンプルは MS1 を 10.8 μL にエポキシ樹脂 180 mg を混ぜ合わせて作成した。液相サンプルは(x,y,z)=(7mm,0mm,0mm)、固相サンプルは(x,y,z)=(21mm,0mm,0mm)を中心として並べて配置した。

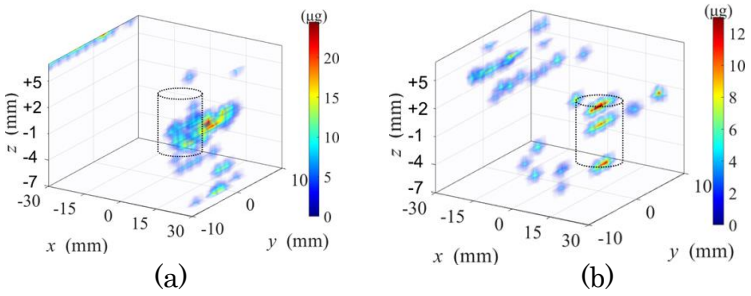

Fig 1. MPI 3D images for (a) liquid sample and (b) solid sample.

Fig 1.に示すように、高調波信号特性を利用することで、状態識別が行えていることが分かる。しかしながら、固相サンプルの一部が液相として識別されていたり、本来サンプルの存在しない位置にアーチファクトが推定されたりしているため、改善は必要である。

参考文献

1) Yoshida, Takashi, et al. "Effect of alignment of easy axes on dynamic magnetization of immobilized magnetic nanoparticles." Journal of Magnetism and Magnetic Materials 427 (2017): 162-167.

セラノスティクス応用に向けたCo-Mg系フェライトのT_2緩和

濱田颯太[1]、坂井直樹[1]、青木孝太[1]、児玉慶太[1]、梨本健太朗[1]、細貝良行[3]、臼井章仁[4]、一柳優子[1,2]
（[1]横国大院、[2]阪大院、[3]国際医療大、[4]東北大）

T_2 relaxation of functional Co-Mg ferrite NPs for theranostics

S.Hamada[1],N.Sakai[1],K.Aoki[1],K.Kodama[1],K.Nashimoto[1],Y.Hosokai[3],A.Usui[4],Y.Ichiyanagi[1,2]
([1]Yokohama Nat. Univ.,[2]Osaka Univ.,[3]Inter. Univ. of Health&Welfare,[4]Tohoku Univ.)

はじめに

我々はこれまでに、さまざまな組成、粒径の磁気ナノ微粒子を作製し、これらの磁気特性の制御と医療応用に向けた研究報告を行ってきた。今回は治療に診断を加えたセラノスティクス応用に向け、Co-Mg系フェライトのMRI造影剤としての機能を検討した。MRI造影剤には使用が禁止されるものもあり、新しい材料開発は喫緊の課題である。本微粒子は、すでに薬剤輸送を意識し、チオール基を修飾しマレイミド系たんぱくを担持することが可能であることも確認している。

実験方法

湿式混合法によりアモルファスSiO_2に包含された$Co_{1-x}Mg_xFe_2O_4$（x = 0.0, 0.2, 0.4, 0.6, 0.8, 1.0）磁気ナノ微粒子を作製した。これらに対して、XRD測定および室温300 Kにおける磁化測定を行った。MRIにおけるT_2緩和測定を、各試料の懸濁液をAgaroseで固化させたファントムを用いて行った。水に対する金属イオン濃度は1.0 mM, Agarose濃度は0.8 wt%である。

実験結果

XRD測定から、各組成において$Co_{1-x}Mg_xFe_2O_4$の単相であり、粒径が約4.5 nmであると算出された。また、2θ = 23°付近のブロードなピークからアモルファスSiO_2による包含が確認された。300 Kにおいては全ての試料でMgドープの増加に伴い磁化が減少し、保磁力は10 Oe以下になった。MRIにおけるT_2緩和測定では、シグナル強度のプロットからフィッティングを行い緩和能R_2 (=1/T_2)を求めた。作製したすべてのサンプルが従来造影剤として用いられる鉄系酸化物よりも緩和率が高く、特にx = 0.2,0.4,0.8のサンプルはγ-Fe_2O_3より約7倍も高い緩和率を示した(Fig.1)。Fig.2にファントム断面のT_2強調画像を示す。Agaroseバックグラウンド（左上）と比較し、作製した試料を含むファントムは、エコー時間TEの経過とともにMRシグナルが減少し、短いTEでも明瞭なコントラストが得られることが確かめられた。これは作製した試料の超常磁性的性質が作用し、微粒子近傍に動的磁場が発生しT_2緩和が促進されたと考えられる。本粒子は官能基修飾も可能にしており、薬剤輸送に加え、診断にも有用なセラノスティクス材料として期待できる。

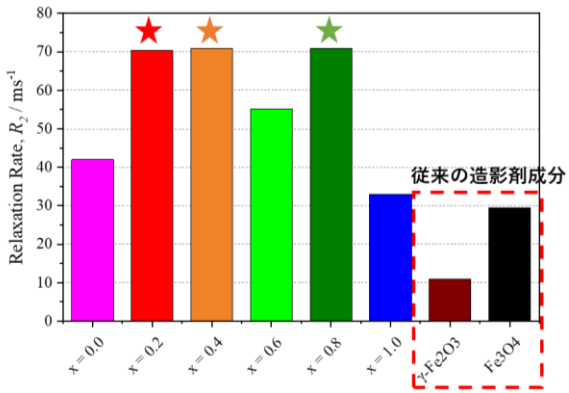

Fig.1 組成別Co-MgフェライトのT_2緩和率

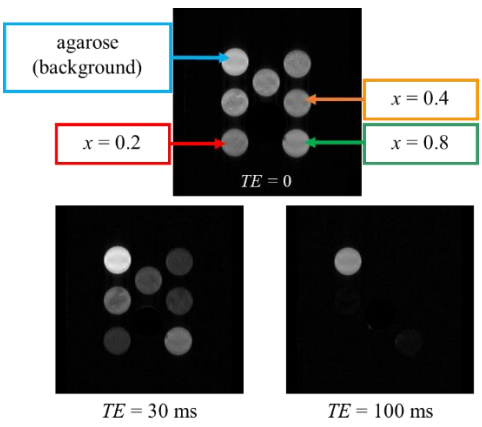

Fig.2 Co-MgフェライトのT_2強調画像

磁気分画したフェルカルボトランの発熱特性

石川真守[1], 大多哲史[2], Suko Bagus Trisnanto[1], 山田努[1], 吉田敬[3],竹村泰司[1]
([1]横浜国立大学, [2]静岡大学, [3]九州大学)

Heat dissipation of magnetically fractionated Ferucarbotran

Mamoru Ishikawa[1], Satoshi Ota[2], Suko Bagus Trisnanto[1], Tsutomu Yamada[1], Takashi Yoshida[3], Yasushi Takemura[1]
([1]Yokohama National Univ., [2]Shizuoka Univ., [3]Kyushu Univ.)

はじめに

磁気ハイパーサーミアにおいて、印加可能な磁場強度・周波数下で磁性ナノ粒子を十分に発熱させることが課題であり、そのために磁性ナノ粒子の磁気特性を解明する必要がある。MRI 造影剤に臨床利用されている Resovist®は粒径分布が広いことが知られており、その原料であるフェルカルボトラン（Ferucarbotran、γ-Fe_2O_3/Fe_3O_4）も同様に広い粒径分布を有する。磁気特性の粒径依存を解明し、特定の磁界強度・周波数での発熱量や、磁気粒子イメージングの検出感度を上げるためには、特定の粒径をもつ磁性ナノ粒子を抽出する手法が有効である。本研究では、フェルカルボトランを特定の粒径群に磁気分画した 3 種類の磁性ナノ粒子を測定試料とした。Specific loss power (SLP)、Intrinsic loss power (ILP)を計算し、粒径依存や磁化容易軸の配向の影響などを明らかにしたので報告する。

実験方法・結果

測定粒子はフェルカルボトラン（Ferucarbotran、γ-Fe_2O_3/Fe_3O_4）を磁気分画した MS1 、MS2、MS3（名糖産業株式会社、コア粒径は MS1：21.6 nm, MS2：10.7 nm, MS3：6.2 nm）[1)]を使用した。それぞれ希釈した液中試料とエポキシ樹脂で固めた固定試料を作製した。固定試料においては、無磁場下で固定した無配向固定試料と 575 kA/m の直流磁場中で固定し粒子の磁化容易軸を揃えた配向固定試料の 2 種類を作製した [2)]。磁性ナノ粒子の濃度は鉄換算として、2 mg-Fe/mL と一定にした。それぞれの試料の直流磁化特性、交流磁化特性（磁場強度 4, 16 kA/m、周波数 1–100 kHz）の測定を行った。配向固定試料は磁化容易軸に対して平行方向と垂直方向に励磁をし、試料の磁化容易軸、磁化困難軸方向の磁化特性を比較した。

Fig. 1 に液中試料（MS1、MS2、MS3）の直流磁化特性、Fig. 2 に交流磁化特性を示す。粒径の大きい順に磁化及び磁気緩和損失が大きくなる [3)]ことが確認できた。当日はこれらの結果の詳細と算出した SLP、ILP に加え、Resovist®との比較等も報告する。

参考文献

1) Yoshida *et al.*, *J. Appl. Phys*., **114**, 173908, 2013
2) Shi *et al.*, *J. Magn. Magn. Master.*, **473**, 148, 2019
3) Sasayama *et al*, *IEEE. Trans. Magn.*, **51**, 5101504, 2015

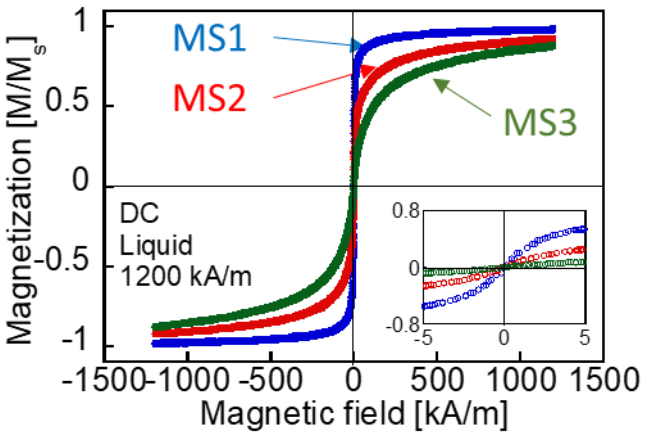

Fig. 1 DC magnetization characteristics of the samples.

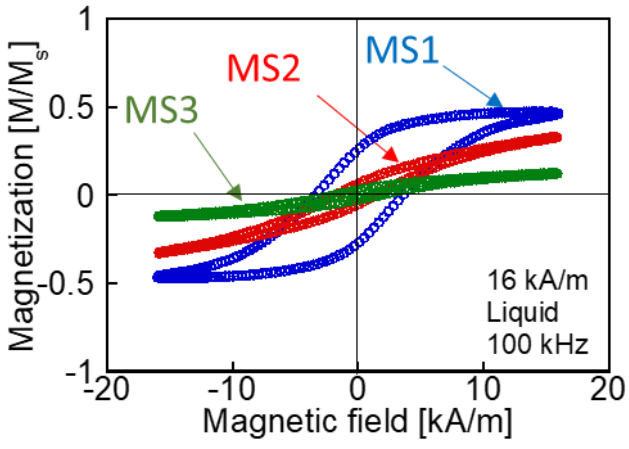

Fig. 2 AC magnetization characteristics of the samples.

Magnetic vortex nanorings の直流・交流磁化特性と発熱特性

笹岡英将[1]、Suko Bagus Trisnanto[1]、山田努[1]、吴交交[2]、成昱[2]、大多哲史[3]、竹村泰司[1]
([1]横浜国立大学、[2]同済大学、[3]静岡大学)

DC/AC magnetization characteristics and heat generation characteristics of Magnetic vortex nanorings

Eisuke Sasaoka[1], Suko Bagus Trisnanto[1], Tsutomu Yamada[1], Jiaojiao Wu[2], Yu Cheng[2], Satoshi Ota[3], Yasushi Takemura[1]
([1]Yokohama National University, [2]Tongji University,China, [3]Shizuoka University)

はじめに

磁性体の医療応用として磁気ハイパーサーミアが挙げられる [1]。磁気ハイパーサーミアは、磁性体の発熱を用いてがん細胞を温め死滅させるがん治療の一種である。本研究では、実際にマウス実験を通して高い発熱量を持つことが確認された磁性体について、その磁化特性と発熱特性を測定した。

実験方法と結果

本研究で測定した試料は、酸化鉄（Fe_3O_4）からなるリング状の磁性材料（Magnetic vortex nanorings）である [2]。この磁性体について、その試料濃度を 2 mg/ml に調整した液中試料及び固定試料（epoxy によって固定）を作製した。直流磁化測定として印加磁界が 1500 mT のメジャーループと、交流磁界による消磁後に 5, 10, 15, 20 mT のマイナーループの測定を行った。また、交流磁化測定として周波数 1, 5, 10, 50, 100 kHz それぞれについて、5, 10, 15, 20 mT での測定を行った。加えて、これらの結果から発熱量を算出した [3]。

Fig. 1, 2 に固定試料の直流磁化測定における、メジャーループ及びマイナーループを示した。Fig.2 のように固定試料の直流磁化特性の結果から、メジャーループでは保磁力と残留磁化が見られ、マイナーループではこれらの値がほとんどないことがわかる。

当日はこの結果についての詳細のほか，固定試料の交流磁化測定，及び液中試料の直流・交流磁化測定と発熱量について報告する。

参考文献

1) Jordan *et al, J.Magn.Mgn.Mater.*, 201, 413, (1999).
2) X Liu *et al, Adv.Mater.*, 27, 1939, (2015).
3) Shi *et al*, *J.Magn.Magn.Master.*, Vol.473, 148, (2019).

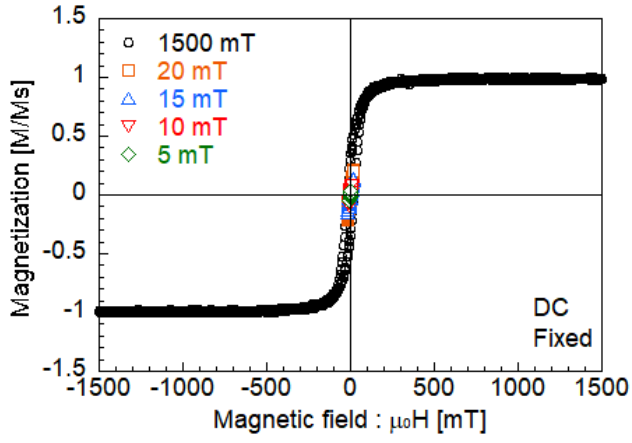

Fig.1 Hysteresis loops of the fixed sample.

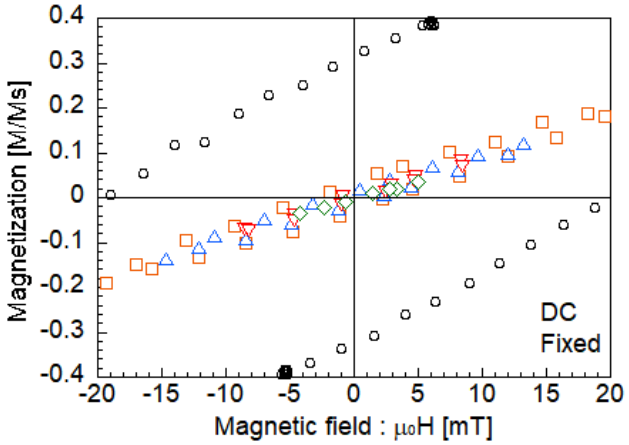

Fig.2 Enlarged view of the hysteresis loops

磁性ナノ粒子の発熱と線形・非線形応答の交流磁化率

山南豪[1], Suko Bagus Trisnanto[1], 山田努[1], 大多哲史[2], 竹村泰司[1]
([1]横浜国立大学, [2]静岡大学)

Heat dissipation of magnetic nanoparticles and the AC susceptibility of their linear and nonlinear responses

Tsuyoshi Yamaminami[1], Suko Bagus Trisnanto[1], Tsutomu Yamada[1], Satoshi Ota[2], Yasushi Takemura[1]
([1]Yokohama National University, [2]Shizuoka University)

はじめに

磁性ナノ粒子を用いた磁気温熱治療[1]において、磁性ナノ粒子の発熱特性を正確に理解する必要がある。本研究では磁性ナノ粒子の特性を示す指標として交流磁化率に着目した。交流磁化率の虚部は磁気損失の指標であり、発熱量Specific loss power(SLP)と相関がある[2]。発熱量の算出に磁化特性が線形領域にある磁化率虚部を用いられることがあるが、実際の温熱治療で用いられる磁場強度・周波数の条件下では磁性ナノ粒子の磁化は非線形応答をする。本研究では磁性ナノ粒子の交流磁化測定をすることにより、試料の非線形性を考慮した磁化率虚部および発熱量との相関を検討した。

実験方法・結果

磁化率虚部の2通りの計算方法をFigure 1に示す。第1の方法(Case1)は、従来の線形理論に基づく印加磁場と磁化の位相差から求める方法である。まず元の交流磁化曲線の印加磁場と磁化の振幅を用いて磁化率の絶対値を求める。次に求めた磁化率の絶対値に印加磁場と磁化の位相差の正弦を乗算することで磁化率虚部χ''_{C1}が求まる。さらにこれらの値から線形な交流磁化曲線が導出され、発熱量が得られる。第2の方法(Case2)は、非線形性を考慮するため交流磁化曲線の面積から求める方法である。まず交流磁化曲線の面積を計算することで発熱量が得られる。次に発熱量の式[2]に代入することにより、磁化率虚部χ''_{C2}を求めることができる。

2通りの方法で求めた異なる磁場強度における磁化率虚部の結果において、低磁場下では試料の磁化が線形応答となるため、計算方法による差がほぼなかったが、高磁場下では計算方法による差が確認できた。これは試料の磁化が高磁場下では非線形応答することに起因する。詳細なデータは当日発表する。

参考文献

1)　A. Jordan, *et al., J. Magn. Magn. Mater.,* **201**, pp.413 (1999).
2)　R.E. Rosensweig *et al., J. Magn. Magn. Mater.,* **252**, pp.370 (2002).

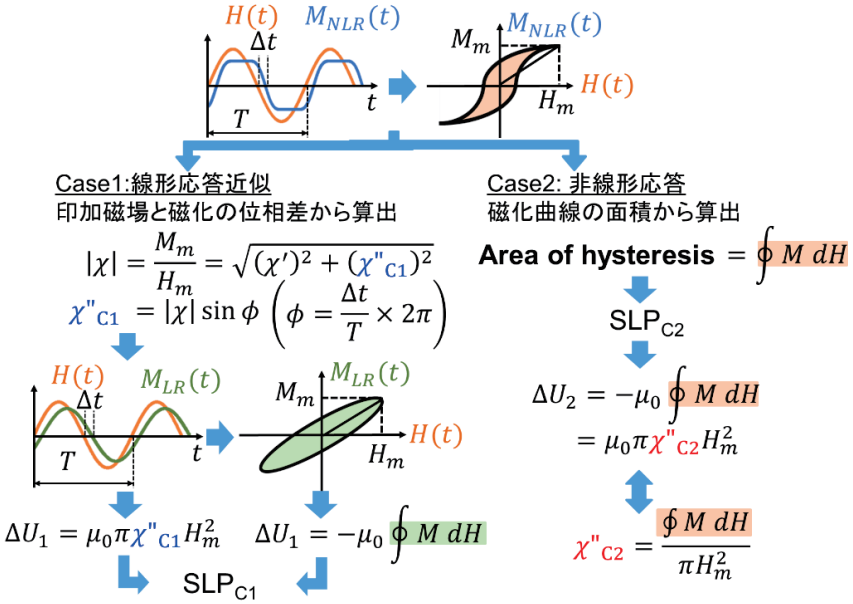

Figure 1 Imaginary part of the AC susceptibility χ'' calculated from the measured AC magnetization curve by linear response approximation (Case1) and nonlinear response (Case2).

磁性ナノ粒子懸濁液の平行・垂直直流磁場下における動的ヒステリシス測定

小野寺礼尚[1]、喜多英治[1,2]、岸本 幹雄[2]、黒岩拓也[2]、柳原英人[2]
([1]茨城高専、[2]筑波大学)
R. Onodera[1], Eiji Kita[1,2], M. Kishimoto[2], T. Kuroiwa[2] and H. Yanagihara[2]
([1]NIT Ibaraki College, [2]Univ. of Tsukuba)

はじめに

近年、磁性ナノ粒子(MNP)は磁気共鳴イメージング(MRI)や磁気ハイパーサーミアなど医療分野への応用が注目されている。磁気ハイパーサーミアでは磁性ナノ粒子分散体に高周波磁場(AMF)を印加した際に発生する熱を癌の焼灼に利用する。発熱剤の材料開発には、MNP の高周波応答、その比損失電力(SLP)および発熱量を評価することが必要となる。

MNP 分散体に直流磁場(DC-MF)を重畳させることで、MNP の運動を制御することができる。ドラッグデリバリーなどの他の治療法と磁気ハイパーサーミアを同時に併用できれば、新たな治療方法の開拓として大きく貢献することができる。直流磁場の重畳は MNP の配向や緩和機構に影響を及ぼすと考えられるため、直流磁場印加時における高周波応答および発熱特性を評価することで効果を明らかにできる。

本研究では、MRI の造影剤として市販されている超常磁性ナノ粒子 Resovist®□と強磁性 Co 置換 Fe_3O_4 ナノ粒子(SCF-3)の懸濁液について、高周波磁場と同時に、平行と垂直な静磁場を印加する装置を開発した。それぞれの試料の動的ヒステリシスを測定し、高周波応答と発熱能に対する静磁場の影響について議論する。

装置構成

本装置は、静磁場発生磁石と AC 磁化測定装置を組み合わせた構成となっている。DC-MF 発生にはφ50mm の磁極を有する電磁石を用い、この磁極間に動的ヒステリシス測定用の AMF 発生コイルおよび、磁化・磁場検出コイルを設置している。DC-MF は磁極中心でおよそ 50 mT の磁場発生が可能となっている。LC 共振回路により、20 k～1 MHz の範囲で交流磁場を空芯コイルに発生させることができる[1)]。DC-MF の磁極と AMF コイルおよび検出コイルの配置を Fig. 1 のように変更することで、平行・垂直双方の DC-MF を重畳させることができる。

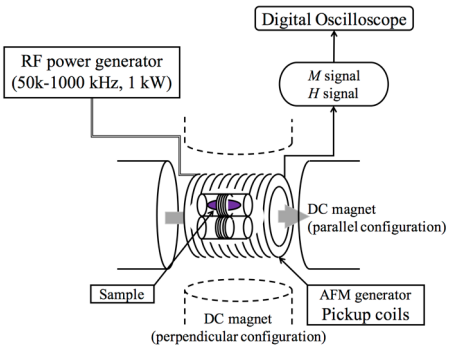

Fig. 1 Schematic configuration of dynamic hysteresis measurement system under parallel and perpendicular DC magnetic fields[2].

実験方法および結果

超常磁性ナノ粒子懸濁液 Resovist®□と強磁性 Co 置換 Fe_3O_4 ナノ粒子懸濁液について、周波数：60-200 kHz、DC-MF：0-50 mT、AMF : 5-70 mT の条件で動的ヒステリシスを測定し、ループ面積から比損失電力(SLP)の DC-MF 依存性を評価した。

測定の結果、AMF に垂直に DC-MF を印加した場合には、平行に DC-MF を印加した場合に比べて、ループ面積が徐々に減少していることがわかった。当日は、サンプルによる DC-MF 依存性の違いと緩和挙動との関連について報告する。

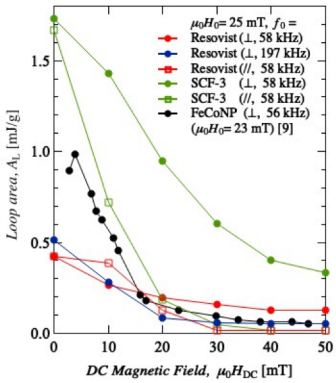

Fig. 2 DC-MF dependence on loop area of dynamic hysteresis loops[2].

参考文献

1) A. Seki, *et al.*, J. Phys.: Conf. Ser., 521 (2014) 012014
2) R. Onodera, *et al.*, IEEE Trans. Mag., *in press*. doi: 10.1109/TMAG.2020.3021428.

磁気ハイパーサーミア用磁場発生装置に生じる磁場と電場の分布

中村 省太、藤枝 俊、清野智史、中川 貴、山本孝夫
（大阪大学 大学院工学研究科）

Distribution of magnetic and electric fields in magnetic circuit type field generator for magnetic hyperthermia

S. Nakamura, S. Fujieda, S. Seino, T. Nakagawa, T. A. Yamamoto
(Graduate school of Engineering, Osaka Univ.)

緒言

磁気ハイパーサーミア療法は、がん細胞周辺に磁性発熱体を注入し、体外から交流磁場を印加することにより発熱させ、がん細胞のみを局所的に加温して死滅させる治療法である。本療法に使用する磁場発生装置は、人体が入る広い範囲に強力な交流磁場を発生させる能力が求められる。本研究グループでは、 実験およびシミュレーションにより対向型励磁コイルを用いた磁場発生装置が、磁極間の比較的広範囲に均一な交流磁場を発生させる方式として有効であることを明らかにしてきた [1]。一方、強力な交流磁場を広範囲に発生させるためには、非常に大きな電流を要するため、強い電場が生じることが懸念される。高周波数帯の電場は人体に対して熱作用を引き起こすことが知られており、磁場発生装置から生じる電場について検討する必要がある。そこで本研究では、50 mm の磁極間距離を持つ磁場発生装置に発生する磁場と電場の分布を明らかにする。

実験方法

磁場発生装置には、E 型フェライトコア（TDK, PC40）を用いた（Fig. 1 参照）。フェライトコアに銅チューブを丸形アクリル筒に 7 巻して励磁コイルを製作した。磁場強度の測定には 10 巻のピックアップコイルを用い、電場強度の測定には電界プローブ（ウェーブクレスト社, FES-100）を用いた。共振周波数は 463 kHz、励磁電流は 1.0 A（最大値）固定とし、測定点を Fig. 1 の磁極中心から y 軸方向に動かしながら測定することで各強度分布を取得した。

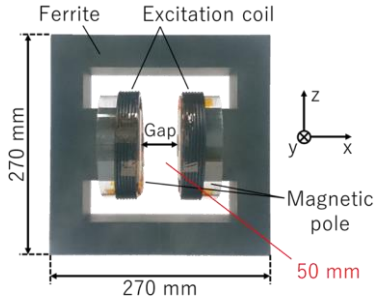

Fig. 1 Magnetic circuit type field generator.

実験結果

Fig. 2 に磁場発生装置に生じる磁場強度および電場強度の実測値を示す。磁場強度の最大値は磁極間で発生し、磁極外では中心からの距離が離れるにつれて減衰していることが確認された。一方、電場強度は磁極外の励磁コイル端近傍で最大（約 370 V/m）となり、磁極間において中心に近づくにつれて減衰していくことが判明した。また、磁極外では電場は磁場と比較して緩やかに減衰する。したがって、対向型励磁コイルを用いた磁場発生装置において、コイル端及び磁極外で人体に対する電場の暴露を抑制する対策を講じる必要があるが、治療時に利用される磁極間は電場による人体への影響が少ないことが明らかになった。

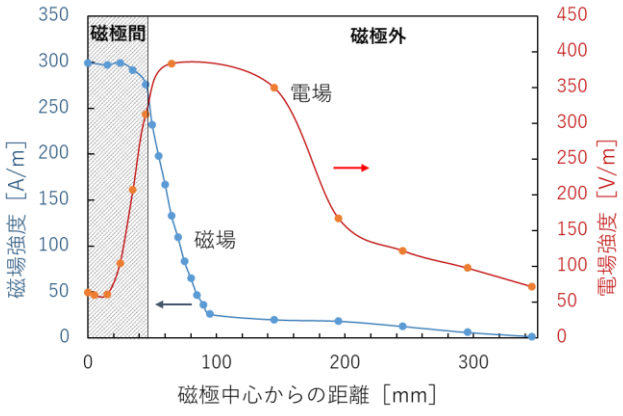

Fig. 2 Distribution of magnetic and electric fields strength.

参考文献

1) K. Sugi, T. Nakagawa, S. Fujieda, S. Seino, T. A. Yamamoto, T. Magn. Soc. Jpn., **4**, 111-115 (2020).

Automated characterization of magnetic materials

Kanta Ono
(Institute of Materials Structure Science, High Energy Accelerator Research Organization (KEK))

Future research and development in magnetic materials requires to focus on the following four essential research areas:

1. Automation of research and development or automated scientific discovery
2. Autonomous robotic technology for research and development
3. AI or machine learning technology for magnetic materials research
4. Data collection, integration, and infrastructure for public access

In this presentation, we will discuss these priority research topics, mainly from magnetic materials' characterization viewpoints. A high-throughput material characterization system with quantum beams, such as X-rays and neutrons, leads to a drastic increase in measurements' speed and efficiency. However, we believe that the essence of material characterization is to extract useful information and knowledge for researchers and to automate the research and development process. Only performing high-throughput measurements and collecting a large amount of measurement data and compiling them into a database is not enough to improve materials research efficiency. We will discuss a methodology to maximize the information obtained per time and cost in the measurement [1-4]. While high-throughput measurements are becoming more common, most of the measurement data analysis is done manually by skilled experts, which is a bottleneck in the efficiency of research and development. In addition to freeing researchers from simple tasks to devote themselves to research activities, the measurement and analysis of data will be commoditized so that anyone can perform the measurement and analysis tasks that were previously performed only by skilled experts.

Reference

1) T. Ueno, H. Hino, A. Hashimoto, Y. Takeichi, M. Sawada, and K. Ono, “Adaptive design of an X-ray magnetic circular dichroism spectroscopy experiment with Gaussian process modelling”, npj Computational Materials 4, 4 (2018).
2) K. Saito, M. Yano, H. Hino, T. Shoji, A. Asahara, H. Morita, C. Mitsumata, J. Kohlbrecher and K. Ono, “Accelerating small-angle scattering experiments on anisotropic samples using kernel density estimation”, Sci. Rep. 9, 1526 (2019)
3) Y. Suzuki, H. Hino, M. Kotsugi and K. Ono, “Automated estimation of materials parameter from X-ray absorption and electron energy-loss spectra with similarity measures” npj Computational Materials 5, 39 (2019).
4) Y. Ozaki, Y. Suzuki, T. Hawai, K. Saito, M. Onishi and K. Ono, “Automated crystal structure analysis based on blackbox optimisation”, npj Computational Materials 6, 75 (2020).

Adaptive design of experiments for X-ray magnetic circular dichroism spectroscopy

Tetsuro Ueno
(Quantum Beam Science Research Directorate, National Institutes for Quantum and Radiological Science and Technology (QST))

X-ray microscopy such as transmission X-ray microscopy (TXM) or scanning transmission X-ray microscopy (STXM) is a modern experimental technique to observe magnetic domains with several ten-nm spatial resolutions. Observation of magnetic domains with these techniques is based on X-ray magnetic circular dichroism (XMCD), a phenomenon that the the absorption coefficient at absorption edges of ferromagnetic materials differs for right- or left-handed circularly polarized X-rays.

We demonstrated the quantitative analysis of magnetic domains with XMCD-STXM [1]. STXM experiment was performed at the Photon Factory, High Energy Accelerator Research Organization [2]. STXM images around Sm $M_{4,5}$ absorption edges of $SmCo_5$ permanent magnet for right- and left-handed circularly polarized X-rays, respectively. X-ray absorption and XMCD spectra were obtained for an area of 2.7×1.4 μm^2 by 100 nm steps. Spatial distributions of spin and orbital magnetic moments were obtained by applying magneto-optical sum rules to pixel-by-pixel XAS and XMCD spectra.

Although XMCD-STXM is a powerful tool to analyze magnetic domains, the experimental throughput is a problem. Typically, it takes several hours to measure one data set. Experimental parameters for STXM are the number of spatial points (scanning area and steps on sample), the number of energy points (energy range and steps), and the dwell time at each point. To improve the efficiency of STXM, we conceived a reduction of energy points using a machine learning technique, Gaussian process regression. We developed an adaptive design of experiments (ADoE) that combines measurement, analysis and machine learning. It is demonstrated that the ADoE for $Sm_{4,5}$ XMCD spectra reduces the energy points to 20% of a conventional experimental design to obtain magnetic moments with satisfactory accuracy [3].

Reference

1) T. Ueno, A. Hashimoto, Y. Takeichi, and K. Ono, “Quantitative magnetic-moment mapping of a permanent-magnet material by X-ray magnetic circular dichroism nano-spectroscopy”, AIP Advances **7**, 056804 (2017).
2) Y. Takeichi, N. Inami, H. Suga, C. Miyamoto, T. Ueno, K. Mase, Y. Takahashi, and K. Ono, “Design and performance of a compact scanning transmission X-ray microscope at the Photon Factory”, Rev. Sci. Instrum. **87**, 013704 (2016).
3) T. Ueno, H. Hino, A. Hashimoto, Y. Takeichi, M. Sawada, and K. Ono, “Adaptive design of an X-ray magnetic circular dichroism spectroscopy experiment with Gaussian process modelling”, npj Computational Materials **4**, 4 (2018).

Coercivity Analysis based on extended Landau free energy landscape

Masato Kotsugi

(Tokyo University of Science)

Microstructure is an important information that characterizes macroscopic function. The coercivity is a typical issue, and we have analyzed the magnetic domain structure and metallographic structure to discuss the origin of macroscopic coercivity. However, a rather problematic approach has been taken for a long time, in which the results of pinpoint local structural analysis are used to discuss the macroscopic function of the entire system. In other words, most of the information of image data has been discarded and the interpretation of the image data required expert knowledges.

Here, we propose a new energy model that can explain macro functions using entire information of microstructure. Spatial inhomogeneity, which could not be dealt with by the Landau model, is quantified and used as a feature using modern mathematical science. Feature extraction combines Persistent homology, Fourier transformation and Ising model to extract significant Physical Feature in multiscale. Selected features are used to draw the free energy landscape that can explain the magnetization reversal process, then analyze the behavior of the saddle point to discuss the origin of macroscopic coercivity. We design the extended Landau energy model that can handle spatial inhomogeneity and explain the macroscopic functions. The model can connect microscopic microstructure and macroscopic materials' function. Furthermore, the modeling the free energy landscape behind the material functions would allow for analysis that goes into the interpretation of the mechanisms. In this talk, we will introduce our recent research projects related to

(1) Feature extraction from magnetic domain structure using Persistent Homology.
(2) Drawing Extended Landau Free Energy Landscape for the analysis of magnetization reversal process and coercivity.

Reference
T. Yamada, M. Kotsugi et al. Vacuum and Surface Science 62, 153, (2019)
https://doi.org/10.1380/vss.62.153

Drawing the extended Landau free energy landscape of polycrystalline magnetic thin films

Alexandre Lira Foggiatto[1*], Sotaro Kunii[1], Chiharu Mitsumata[2] and Masato Kotsugi[1]
([1]Tokyo University of Science, [2]NIMS)

The understanding of the function of real materials in a heterogeneous system, such as magnetic domain and metallographic structure, has been an outstanding issue in materials science. Thus the development of a consistent and fast analysis method that considers the defects, roughness, crystal sizes, etc. is of utmost importance.[1)] Here, we are developing a machine learning-based formula that can treat the microscopic morphology and describes the macroscopic properties based on the energy of the system. One important application is to describe the coercivity based on the structure and micromagnetic properties.[2)] The Landau free energy theory is arduous to be implemented in complex applications due to the pinning de-pinning process of the domain walls.[3)] Thus, the description of the physics in inhomogeneous polycrystalline systems considering the metallography structure is necessary for advanced material applications.

In this work, we use micromagnetic simulation to calculate the external field dependence of magnetization in polycrystalline permalloy (Fig. 1) and analyze it using unsupervised machine learning to find correlations between the images in the data set. The energy landscape in the magnetization reversal process is successfully visualized as a function of features (Fig. 2). It is an observed correlation between the reduced feature space and the hysteresis loop. The map of the data in lower dimension space of the magnetization, in the same direction of the external magnetic field, displays a clear coercivity dependence. Small grains sizes have smaller components and broader distribution in the feature space, which is inverse proportion to the coercivity. Moreover, the landscape map allows us to access and predict the total energy of the system. Our result implies that the magnetic microstructure can display information about the macroscale properties.

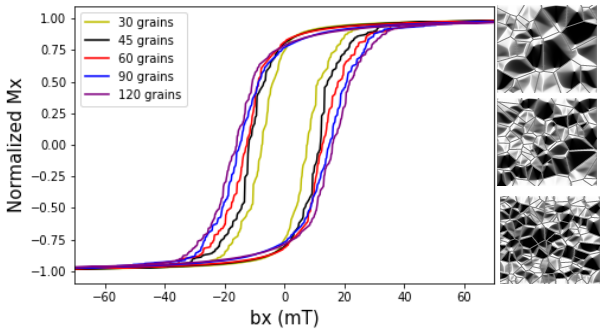

Fig. 1. Hysteresis loop for different grain sizes and magnetic domain structures near coercivity for 30, 60 and 120 grains.

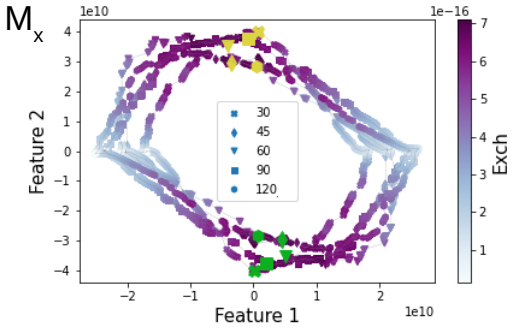

Fig. 2. Reduced feature space of the magnetization reversal process of the x components. The green an yellow points correspond to the positive and negative coercivity.

Reference

1) C. Shen, et al., Acta Materialia **179**, 201 (2019).
2) C. H. Chen, et al., J. Appl. Phys. **93**, 7966 (2003)
3) A. Hubert, R. Schäfer “Magnetic Domains: The Analysis of Magnetic Microstructures” (Springer-Verlag, Berlin, Heidelberg, 1998).

Precision improvement in electron holography: application of information science to magnetic structure analysis

Y. Murakami[1], T. Tanigaki[2], H. Shinada[2] and Y. Midoh[3]
1 Department of Applied Quantum Physics and Nuclear Engineering, Kyushu University, Fukuoka 819-0395, Japan.
2 Research & Development Group, Hitachi, Ltd., Hatoyama 350-0395, Japan.
3 Graduate School of Information Science and Technology, Osaka University, Suita 565-0871, Japan.

Electron holography, which is a method related to transmission electron microscopy (TEM), can be a tool for the magnetic domain structure analysis, as it enables magnetic flux mapping in a nanometer-scale resolution. Actually, some of the authors [1)] have attained the atomic-scale resolution in the flux mapping from an oxide crystal, as it will be briefly mentioned in this symposium. For the applications to materials science and engineering, the other essential factor is “precision” of the magnetic flux density measurement. Importantly, the precision of electron holography depends on the image quality of “hologram” which is made of interference fringes of the incident electrons. (The hologram provides information about the phase shift of the incident electrons which traverse a magnetic specimen.) Although a long-time electron exposure can be an effective way to improve the image quality of holograms, it induces undesired specimen drift during data collection, surface contaminations, radiation damage, and other such problems. We have employed several techniques of information science and/or data science to improve the image quality of holograms. An essential technique is of noise reduction from holograms which were collected in a short exposure time (to suppress the undesired events caused by a long-time exposure). Midoh *et al.* [2)] introduced Markov property into the process of noise reduction using the wavelet transform and thresholding. Based on this modeling, they established a criterion for the separation of noise from weak signal in the holograms. The noise reduction improved the precision in phase analysis by 4-5 times as compared with the value from the original (unprocessed) hologram. In addition to this modeling, for another route of the noise reduction, we employed machine learning and the other methods of image processing to carry out the averaging of many holography observations.

Electron holography was applied to the magnetic flux density measurement from a narrow grain boundary produced in a 0.1% Ga-doped Nd-Fe-B sintered magnet [3)]. Because of the methods of precision improvement, the uncertainty in phase detection was reduced to $2\pi/210$ rad. The result is better than the value ($2\pi/80$ rad) attained in the previous electron holography study which revealed the presence of ferromagnetic grain boundaries in a commercial Nd-Fe-B magnet subjected to the optimal heat treatment [4)]. A sophisticated electron holography study [3)] allowed the magnetic flux density measurements as a function of positions along the grain boundary region: see Fig. 1. The observations provide useful information about the magnetic and/or chemical inhomogeneity in the grain boundary region in the 0.1% Ga-doped Nd-Fe-B magnet.

The authors are grateful to Drs. K. Hono, T. Ohkubo, and T. Sasaki (NIMS) for their collaborations with the study of the 0.1% Ga-doped Nd-Fe-B magnet. This study was supported by CREST (JPMJCR1664) and ESICMM (JPMXP0112101004). A part of the study was supported by FIRST Program initiated by CSTI.

Reference

1) T. Tanigaki *et al.,* manuscript in preparation.
2) Y. Midoh *et al.,* Microsc. **69** (2020) 121.
3) Y. Cho *et al.,* Scripta Mater. **178** (2020) 533.
4) Y. Murakami *et al.,* Acta Mater. **71** (2014) 370.

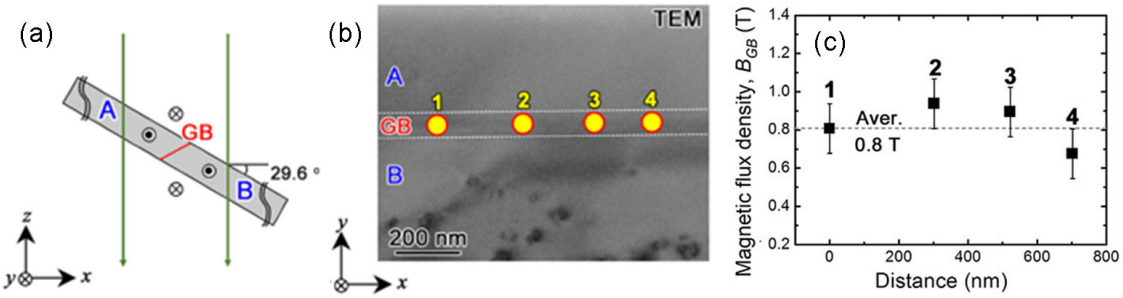

Fig. 1 Magnetic flux density measurements from the grain boundary (GB) in 0.1% Ga-doped Nd-Fe-B sintered magnet. (a) Schematic representation of the cross-section of thin-foil specimen, made of two $Nd_2Fe_{14}B$ grains A and B. (b) TEM image of the thin-foil specimen. Since the plane of GB was tilted away from the incident electron, the projection provides a wide GB region (~90 nm): refer to the area indicated by the white lines. (c) Magnetic flux density measurements from the points 1-4 in (b).